

# Along-Arc and Back-Arc Attenuation, Site Response, and Source Spectrum for the Intermediate-Depth 8 January 2006

## M 6.7 Kythera, Greece, Earthquake

by David M. Boore, Andreas A. Skarlatoudis, Basil N. Margaris, Costas B. Papazachos, and Chrisa Ventouzi

**Abstract** An M 6.7 intermediate-depth (66 km), in-slab earthquake occurring near the island of Kythera in Greece on 8 January 2006 was well recorded on networks of stations equipped with acceleration sensors and with broadband velocity sensors. All data were recorded digitally using recording instruments with resolutions ranging from almost 11 to 24 bits. We use data from these networks to study the distance dependence of the horizontal-component Fourier acceleration spectra (FAS) and horizontal-component pseudoabsolute response spectral acceleration (PSA). For purposes of simulating motions in the future, we parameterize the distance decay using several forms of the geometrical-spreading function, for each of which we derive  $Q$  as a function of frequency. By extrapolating the distance decay back to 1 km, we obtain a reference spectrum that can be used in future simulations. This spectrum requires a more complicated spectral shape than the classic single-corner-frequency model; in particular, there appears to be an enhancement of motion around 0.2–0.3 Hz that may be due to the radiation of a 3–5 sec pulse from the source. We infer a  $\kappa_0$  value of about 0.055 sec for rock stations and a stress parameter in the range of 400–600 bars. We also find distinctive differences in the site response of stations on soft soil and soil; both the FAS and the 5% damped PSA amplifications have similar peak amplitudes (about 2 and 4 for soil and soft-soil sites, respectively, relative to the rock sites) at similar frequencies (between about 0.4 and 2.0 Hz, with the soft-soil amplifications peaking at somewhat lower frequencies than the soil amplifications). One of the most distinctive features of the data is the clear difference in the motions for along-arc and back-arc stations, with the former being significantly higher than the latter over a broad range of frequencies at distances beyond about 250 km. The motions from the Kythera earthquake are roughly comparable to those from intermediate-depth earthquakes elsewhere, but they appear to be significantly higher than those from recordings of shallow earthquakes in Greece of comparable magnitude and hypocentral distance.

### Introduction

The Kythera intermediate-depth earthquake (M 6.7, depth = 66 km) occurred in the western part of the Hellenic arc (Fig. 1; Table 1). No other Greek intermediate-depth earthquakes, including recent ones in 2007 and 2008, have produced a dataset of ground shaking that is at all comparable, in terms of abundance and quality, to that from the Kythera earthquake. The earthquake produced extensive damage in the village of Mitata, in the middle of Kythera Island (Earthquake Engineering Research Institute [EERI], 2006; Karakostas *et al.*, 2006). Because of its magnitude and wave-propagation properties in the subducting slab,

the earthquake was strongly felt throughout Greece and in a very large area of the Eastern Mediterranean region, from central and southern Italy and Albania to Egypt and Jordan.

Intermediate-depth earthquakes along the Hellenic arc occur along a well-defined Wadati–Benioff zone, which has a more or less amphitheatrical shape, at depths ranging from about 60 to 170 km. The Wadati–Benioff zone is due to the subduction of the Eastern Mediterranean lithosphere under the Aegean microplate (Papazachos and Comninakis, 1969; LePichon and Angelier, 1979). The subducting slab

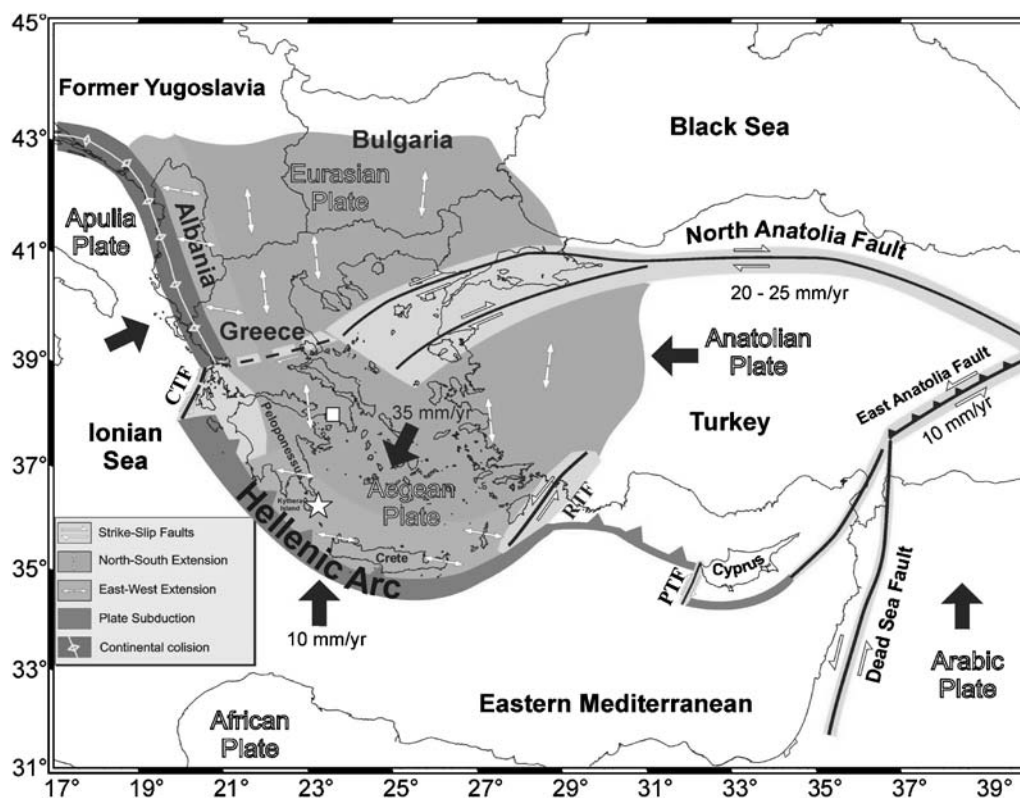


**Figure 1.** Plate motions that affect active tectonics in the Aegean and surrounding area (modified from Papazachos *et al.*, 1998). The epicenter of the Kythera earthquake is shown by the star between the Peloponnese Peninsula and Crete; the square is the epicenter of the 1964 Athens intermediate-depth earthquake (see also Fig. 3). CTF, RTF, and PTF are transform faults.

dips at a relatively low angle (20°–30°) up to the depth of ~90 km and then changes dip to ~45° at larger depths, as is recognized from both the Wadati–Benioff-zone geometry and the available 3D tomographic images (Hatzfeld *et al.*, 1988; Papazachos and Nolet, 1997; Papazachos *et al.*, 2000). While shallow events ( $h < 50$  km) along the Hellenic arc are typical low-angle thrust events due to an almost horizontal northeast–southwest compression (Papazachos and Delibasis, 1969), intermediate-depth events are strike-slip events with a significant thrust component (e.g., Taymaz *et al.*, 1990). This faulting pattern is in accordance with the observed along-arc horizontal compression and the down-dip extension along the subducted slab (Kiratzi and Papazachos, 1995). The Kythera earthquake focal mechanism, computed by the inversion of teleseismic waveforms, shows primarily reverse slip with a strike-slip component along a northeasterly striking plane (strike, 50°; dip, 55°; rake, 115°) (Beneatatos and Kiratzi, 2006) (Fig. 2), due to northwest–southeast

compression following the local trend of the Hellenic arc and northeast–southwest down-dip extension, parallel to the dip of the subducting slab. This result is in very good agreement with existing results, both regarding the typical fault characteristics predicted for this area by Papazachos and Papazachou (2003) (typical fault D2 in their study; strike, 61°; dip, 70°; rake, 144°), as well as the previously described stress field for in-slab intermediate-depth events.

Intermediate-depth earthquakes in the Hellenic subduction zone are characterized by significant differences in along-arc and back-arc attenuation (e.g., Papazachos and Comninakis, 1971). This phenomenon is more pronounced as the depth of the intermediate-depth event increases. Several large-depth events (depths between 100 and 160 km) were not felt at all in the back-arc epicentral area above the hypocenter but caused significant damage at large epicentral distances (>200 km) along the Hellenic arc (these events include the Athens earthquake, 17 July 1964,

Table 1

Earthquake Information (from the Seismological Station of Aristotle University, Thessaloniki, Greece)

Name	Date	Origin Time	Epicenter: Latitude	Epicenter: Longitude	Depth	M
Kythera	8 January 2006	11:35 GMT	36.311° N	23.212° E	66 km	6.7

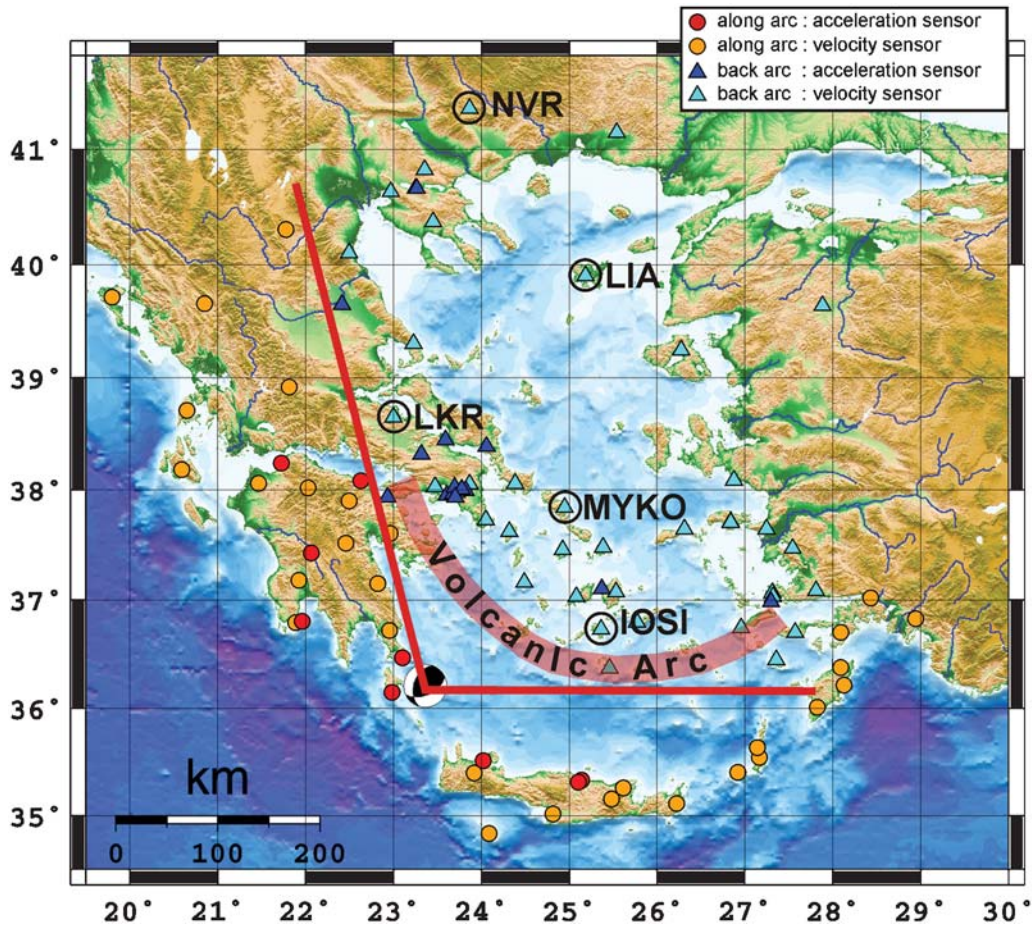


**Figure 2.** Acceleration-sensor and velocity-sensor stations used in the analysis presented in this article. The along-arc, back-arc classification is based on judgment developed by considering seismotectonic properties of the broader Aegean area (see Fig. 1); the red lines, at azimuths of  $-10^\circ$  and  $90^\circ$ , approximately divide the stations into along- and back-arc regions. The labeled stations enclosed with circles are those with unusually low motions, especially at low frequencies; the motions from these stations were excluded from the analysis (see text).

$h = 155$  km,  $M$  6.0 and the Milos earthquake, 21 May 2002,  $h = 107$  km,  $M$  5.9).

Travel-time tomographic results (Spakman, 1988; Spakman *et al.*, 1993; Papazachos and Nolet, 1997) suggest that low compressional-wave and shear-wave velocities ( $V_P$  and  $V_S$ ) values are found at the Aegean mantle wedge, above the subducting slab. There is increased shear-wave damping, as characterized by low values of  $Q_S$ , as well. This low-velocity, attenuating wedge is probably the result of the dehydration of hydrous minerals from the subducted plate at the depth of  $\sim 80$  km. As the released water propagates upward, the mantle wedge above the subducting slab is enriched with water, resulting in partial melting and significant reduction of velocity and quality-factor values. Notice that this melting does not occur within the subducting slab, as typical slab temperatures ( $T \sim 500^\circ\text{--}700^\circ$ ) are much lower than in the corresponding mantle wedge temperatures ( $T > 1000^\circ\text{C}$ ); as a result, the subducting slab forms a high velocity–high quality-factor channel in the surrounding mantle. Moreover, the slab dehydration and the resulting density increase are in good correlation with the previously men-

tioned change in dip of the slab and the Wadati–Benioff zone at the depth of  $\sim 90$  km, as well as the position of the Hellenic volcanic arc (Papazachos *et al.*, 2005), as a surface manifestation of the partial melt (Fig. 2).

Figure 3 schematically illustrates how this structural pattern of the low velocity–low  $Q$  mantle wedge controls the waveform characteristics for intermediate-depth earthquakes. For shallower intermediate-depth events ( $h \sim 60\text{--}70$  km), such as the Kythera event, only rays traveling at relatively large epicentral distances in the back-arc area (such as the subhorizontal dashed line in the figure) are attenuated by the high anelastic attenuation of the mantle wedge. On the other hand, for the deeper intermediate-depth events ( $h \sim 150$  km), such as the 1964 Athens earthquake, all waves traveling in the back-arc area are highly attenuated in the mantle wedge. Furthermore, guided waves traveling upwards along the high velocity–high  $Q$  channel of the slab (thick solid rays in Fig. 3) may even exhibit additional amplification in the along-arc stations. Notice that the mantle wedge attenuation effect is stronger for the  $S$ -wave segment of the waveform because the partial melt, estimated from petrogenetic results (Zelimer,

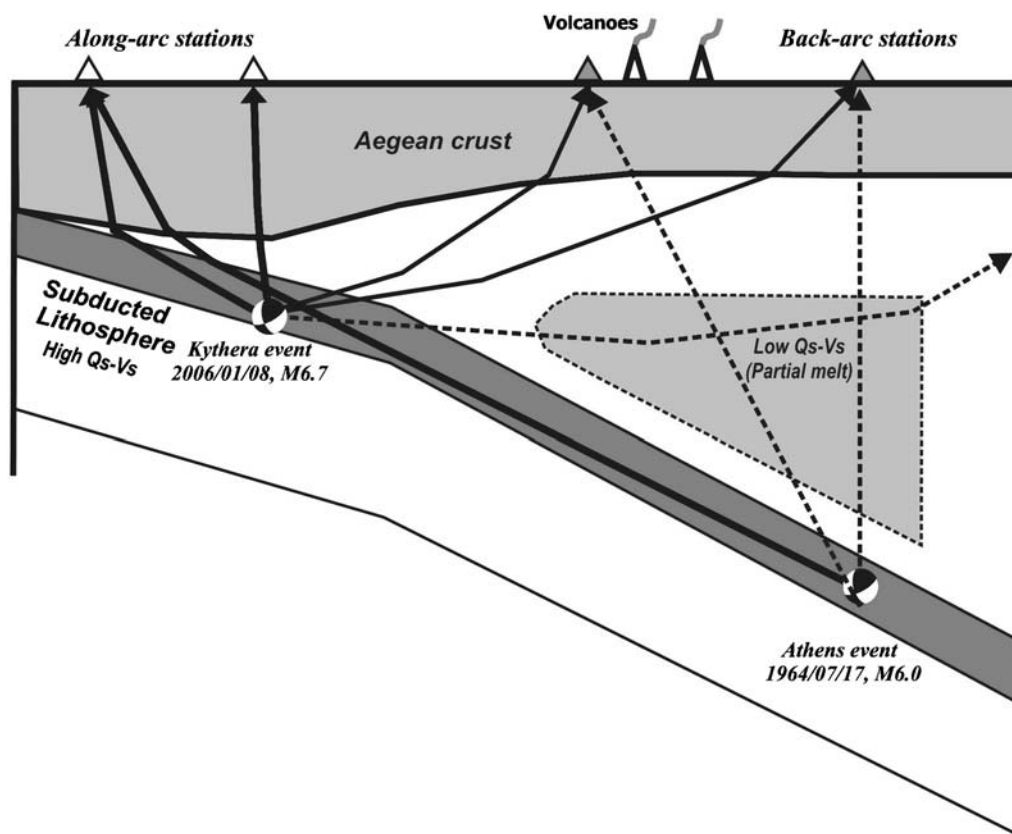


**Figure 3.** Schematic presentation of the wave propagation for intermediate-depth events in the Hellenic arc. Dashed and solid lines correspond to rays that penetrate or do not penetrate the low  $Q_S - V_S$  mantle wedge, respectively, while thick solid lines correspond to rays traveling through the high  $Q_S - V_S$  subducting slab. The focal mechanism plots are those that would be plotted on a map (using the standard projection to a horizontal surface).

1998) and seismological constraints (Karagianni *et al.*, 2005) is estimated to locally exceed 15%, thus affecting mostly  $S$  velocities and  $Q_S$  values. The influences of the slab structure and the low- $Q$  mantle wedge are similar to that observed in Japan, as discussed in a number of articles, including an early article by Fukushima (1997).

Despite the fact that several empirical prediction studies have been made for subduction zones worldwide (Crouse, 1991; Youngs *et al.*, 1997; Gregor *et al.*, 2002; Atkinson and Boore, 2003; Kanno *et al.*, 2006; Zhao *et al.*, 2006; Aguirre and Irikura, 2007, among others), the only study of this type for the Greek subduction zone was performed by Theodulidis and Papazachos (1990) with the use of strong-motion data from similar seismotectonic regions worldwide.

Skarlatoudis *et al.* (2009) studied peak accelerations and peak velocities for the Kythera earthquake. Our article is a major expansion of their study. We perform regression fits of Fourier acceleration spectra (FAS) and pseudoabsolute response spectral acceleration (PSA) to obtain frequency-dependent attenuation parameters and site amplifications, in addition to constraints on the source spectrum for the earthquake.

We start with a discussion of the data sources and the properties of the data, before turning to a regression analysis

of the FAS. This is followed by a brief discussion of results from a regression fit to PSA, after which we have a section comparing the motions to those from other intermediate-depth earthquakes.

#### Data Sources and Instrument Information

We use data from many sources, including both seismological and acceleration-sensor networks deployed in the broader Aegean area (Table 2; more information can be found in Skarlatoudis *et al.* [2009], and in the section on [Data and Resources](#)). All the velocity-sensor data that we will use in our analysis have been recorded by broadband velocity sensors (typically with a flat-to-velocity response from 60 sec to 50 Hz and 18 to 24 bit dataloggers). We use the term “velocity-sensor data” to mean “broadband velocity-sensor data.” All of the accelerometer data were recorded digitally, using lower-resolution dataloggers (typically 11 bit) than used for the velocity data. We note that the majority of recordings were on rock sites.

We are fortunate that the Kythera earthquake occurred while the EGELADOS stations were deployed (the network ceased operation sometime during 2006) and after many stations of the permanent seismological networks had installed broadband sensors with high-resolution digital recording,

Table 2  
Information for Data Used in the Article

Station	SPS <sup>a</sup>	f <sub>0</sub> <sup>b</sup>	f <sub>c</sub> <sup>c</sup>	Latitude (°)	Longitude (°)	R <sub>HYP</sub> <sup>d</sup>	AZ <sup>e</sup>	Institute <sup>f</sup>	Sensor <sup>g</sup>	ARC <sup>h,i</sup>	SOIL <sup>j,k</sup>	SSOIL <sup>l</sup>	PGA <sup>m</sup>
KYT1	200	DC	0.05	36.15	22.983	71	-95	ITSAK	1	1	0	0	120.70
ANS1	200	DC	0.1	36.472	23.101	73	-40	ITSAK	1	1	0	0	144.30
VLI	50	0.05	0.05	36.72	22.95	94	-34	HL	0	1	0	0	14.04
HAN1	200	DC	0.1	35.518	24.019	110	143	ITSAK	1	1	0	1	41.38
KARN	20	0.05	0.05	35.402	23.917	116	152	GEOFON	0	1	0	0	41.36
PE07	100	0.01	0.05	37.148	22.82	133	-26	EGELADOS	0	1	0	0	51.10
SERI	100	0.01	0.05	37.161	24.485	157	41	EGELADOS	0	0	0	0	28.38
KRN1	200	DC	0.14	36.802	21.961	158	-61	ITSAK	1	1	1	0	25.09
PE09	100	0.01	0.05	36.792	21.888	163	-63	EGELADOS	0	1	0	0	12.97
GVD	20	0.05	0.05	34.839	24.087	173	157	GEOFON	0	1	0	0	12.10
PE04	100	0.01	0.05	37.601	22.959	173	-14	EGELADOS	0	1	0	0	13.82
PE05	100	0.01	0.05	37.513	22.455	180	-29	EGELADOS	0	1	0	0	5.59
ITM	50	0.05	0.05	37.179	21.925	182	-49	HL	0	1	0	0	7.17
PE06	100	0.01	0.05	37.179	21.925	182	-49	EGELADOS	0	1	0	0	7.02
ANPA	100	0.01	0.05	37.032	25.076	186	57	EGELADOS	0	0	0	0	7.53
KEAI	100	0.01	0.05	37.623	24.319	189	27	EGELADOS	0	0	0	0	15.15
AT04	100	0.01	0.05	37.725	24.05	190	18	EGELADOS	0	0	0	0	10.71
HER1	200	DC	0.2	35.318	25.102	191	121	ITSAK	1	1	1	0	49.85
SIVA	20	0.05	0.05	35.018	24.81	191	135	GEOFON	0	1	0	0	12.85
MEGA	200	DC	0.05	37.427	22.06	192	-40	PPC	1	1	0	1	9.22
IOSI	100	0.0083	0.05	36.735	25.362	195	70	EGELADOS	0	0	0	0	3.60
SANT	20	0.05	0.05	36.371	25.459	195	83	GEOFON	0	0	0	0	13.91
HER2	200	DC	0.08	35.338	25.136	197	120	ITSAK	1	1	0	1	31.35
ATHC	200	DC	0.14	37.931	23.698	205	8	GEIN-NOA	1	0	1	0	17.17
SYRO	100	0.01	0.05	37.457	24.927	205	43	EGELADOS	0	0	0	0	10.50
KERA	200	DC	0.08	37.953	23.607	206	5	PPC	1	0	1	0	15.62
KORA	200	DC	0.14	37.93	22.93	207	-12	GEIN-NOA	1	0	0	1	23.58
RNTA	200	DC	0.14	37.96	23.68	208	7	GEIN-NOA	1	0	0	1	25.79
ATH	50	0.05	0.1	37.972	23.717	209	8	HL	0	0	0	0	12.26
NAX1	200	DC	0.05	37.1	25.367	211	59	ITSAK	1	0	1	0	3.00
ATHA	200	DC	0.1	38.001	23.774	213	9	GEIN-NOA	1	0	1	0	11.08
DMKA	200	DC	0.14	37.99	23.82	213	10	GEIN-NOA	1	0	0	0	11.22
AT03	100	0.01	0.05	38.027	23.468	214	2	EGELADOS	0	0	0	0	6.36
PRSA	200	DC	0.14	38.02	23.69	214	7	GEIN-NOA	1	0	1	0	19.75
PE02	100	0.01	0.05	37.896	22.491	215	-23	EGELADOS	0	1	0	0	13.07
AT02	100	0.01	0.05	38.047	23.864	219	11	EGELADOS	0	0	0	0	9.48
APE	20	0.05	0.05	37.069	25.531	222	62	GEOFON	0	0	0	0	4.19
LAST	20	0.05	0.05	35.161	25.479	227	121	GEOFON	0	1	0	0	7.00
AMOS	100	0.01	0.05	36.796	25.769	230	71	EGELADOS	0	0	0	0	4.84
XLCA	200	DC	0.14	38.08	22.63	230	-18	GEIN-NOA	1	1	0	1	25.61
NPS	50	0.05	0.05	35.263	25.613	232	116	HL	0	1	0	0	11.24
AT01	100	0.01	0.05	38.056	24.378	233	22	EGELADOS	0	0	0	0	12.07
MYKO	100	0.0083	0.05	37.482	25.384	236	50	EGELADOS	0	0	0	0	2.44
ANDR	100	0.01	0.05	37.836	24.948	237	36	EGELADOS	0	0	0	0	6.63
PE01	100	0.01	0.05	38.017	22.028	245	-30	EGELADOS	0	1	0	0	5.66
THVC	200	DC	0.14	38.32	23.318	245	-2	GEIN-NOA	1	0	1	0	12.87
1M41	200	DC	0.1	38.447	23.592	259	4	ITSAK	1	0	0	0	6.54
4M71	200	DC	0.1	38.447	23.592	259	4	ITSAK	1	0	0	0	7.49
ALIB	200	DC	0.1	38.388	24.053	259	13	PPC	1	0	1	0	4.75
RLS	50	0.05	0.05	38.058	21.467	277	-39	HL	0	1	0	0	3.35
PATB	200	DC	0.14	38.24	21.72	279	-33	GEIN-NOA	1	1	0	1	11.72
LKR	50	0.033	0.05	38.651	22.999	283	-7	HL	0	0	0	0	2.29
ZKR	20	0.05	0.05	35.115	26.217	287	114	GEOFON	0	1	0	0	3.82
IKAR	100	0.01	0.05	37.644	26.305	311	57	EGELADOS	0	0	0	0	1.83
KOSI	100	0.01	0.05	36.745	26.952	329	78	EGELADOS	0	0	0	0	2.85
KASO	100	0.01	0.05	35.412	26.915	334	104	EGELADOS	0	1	0	0	5.35
VLS	50	0.05	0.05	38.177	20.59	339	-47	HL	0	1	0	0	6.82
EVR	50	0.05	0.05	38.917	21.809	340	-24	HL	0	1	0	0	2.17
KAPA	100	0.01	0.05	35.64	27.138	347	99	EGELADOS	0	1	0	0	5.70
NEO	50	0.05	0.05	39.307	23.224	353	-3	HL	0	0	0	0	1.58

(continued)

Table 2 (Continued)

Station	SPS <sup>*</sup>	f0 <sup>†</sup>	fc <sup>‡</sup>	Latitude (°)	Longitude (°)	R <sub>HYP</sub> <sup>§</sup>	AZ <sup>  </sup>	Institute <sup>#</sup>	Sensor <sup>**</sup>	ARC <sup>††</sup>	SOIL <sup>‡‡</sup>	SSOIL <sup>‡‡</sup>	PGA <sup>§§</sup>
SAMO	100	0.01	0.05	37.704	26.838	354	60	EGELADOS	0	0	0	0	0.96
SMG	50	0.05	0.05	37.709	26.837	354	60	HL	0	0	0	0	0.98
TILO	100	0.01	0.05	36.449	27.354	360	84	EGELADOS	0	0	0	0	3.09
KOS1	200	DC	0.1	36.983	27.29	363	74	ITSAK	1	0	1	0	2.06
BODT	50	0.033	0.05	37.062	27.31	367	73	KO	0	0	0	0	0.75
TUR5	100	0.01	0.05	37.03	27.317	367	74	EGELADOS	0	0	0	0	0.69
LKD	100	0.05	0.05	38.707	20.651	376	-40	THENET	0	1	0	0	7.43
TUR1	100	0.01	0.05	38.087	26.868	378	54	EGELADOS	0	0	0	0	0.58
TUR2	100	0.01	0.05	37.642	27.242	382	63	EGELADOS	0	0	0	0	0.45
TUR7	100	0.01	0.05	36.702	27.57	382	80	EGELADOS	0	0	0	0	0.73
S1	200	DC	0.1	39.646	22.409	399	-12	Astronomical Obs.	1	0	0	1	3.37
TUR3	100	0.01	0.05	37.466	27.538	399	67	EGELADOS	0	0	0	0	1.72
RODS	100	0.01	0.05	36.012	27.82	402	91	EGELADOS	0	1	0	0	3.16
TUR4	100	0.01	0.05	37.08	27.808	410	74	EGELADOS	0	0	0	0	1.31
RODN	100	0.01	0.05	36.38	28.084	424	86	EGELADOS	0	1	0	0	2.94
TUR9	100	0.01	0.05	36.702	28.089	427	81	EGELADOS	0	1	0	0	1.95
ARG	50	0.05	0.05	36.216	28.126	428	88	HL	0	1	0	0	3.03
PRK	50	0.05	0.05	39.246	26.272	428	36	HL	0	0	0	0	0.47
LIA	50	0.033	0.05	39.898	25.183	445	20	HL	0	0	0	0	0.13
LIT	100	0.01	0.05	40.101	22.49	447	-10	THENET	0	0	0	0	0.91
JAN	50	0.05	0.05	39.657	20.851	450	-29	HL	0	1	0	0	3.49
TUR6	100	0.01	0.05	37.016	28.426	462	77	EGELADOS	0	1	0	0	0.70
PLG	50	0.05	0.05	40.374	23.446	470	0	HL	0	0	0	0	0.29
KZN	50	0.05	0.05	40.307	21.771	484	-17	HL	0	1	0	0	1.94
THE	100	0.01	0.05	40.633	22.966	500	-4	THENET	0	0	0	0	0.18
W021	200	DC	0.08	40.661	23.26	501	-1	ITSAK	1	0	0	1	2.24
W031	200	DC	0.08	40.66	23.251	501	-1	ITSAK	1	0	0	1	1.77
TUR8	100	0.01	0.05	36.827	28.939	503	80	EGELADOS	0	1	0	0	2.31
KEK	50	0.05	0.05	39.713	19.799	507	-38	HL	0	1	0	0	4.21
SOH	100	0.01	0.05	40.822	23.354	519	0	THENET	0	0	0	0	0.32
NVR	50	0.033	0.05	41.35	23.862	579	4	HL	0	0	0	0	0.03
RDO	50	0.05	0.07	41.146	25.538	585	18	HL	0	0	0	0	0.08

<sup>\*</sup>SPS is samples per sec.

<sup>†</sup>f0 is the sensor frequency.

<sup>‡</sup>fc is the low-cut filter frequency.

<sup>§</sup>R<sub>HYP</sub> is the hypocentral distance.

<sup>||</sup>AZ is the source-to-station azimuth.

<sup>#</sup>Definitions: HL, Geodynamic Institute of the National Observatory of Athens; THENET, Seismological Station of Aristotle University of Thessaloniki; EGELADOS, temporary seismological network deployed in the Southern Aegean area, coordinated by the Ruhr-University of Bochum (Germany) and operated by a large working group involving University of Thessaloniki, National Observatory of Athens, Technical University of Chania (Greece), Istanbul Technical University (Turkey), University of Hamburg and GeoForschungszentrum Potsdam (Germany); GEOFON, GeoForschungszentrum in Potsdam; KO, Kandilli Observatory and Earthquake Research Institute (KOERI); ITSAK, Institute of Engineering Seismology and Earthquake Engineering; PPC, Public Power Corporation; GEIN-NOA, Geodynamic Institute of the National Observatory of Athens; Astronomical Obs., instrument operated by the Larissa Astronomical Observatory.

<sup>\*\*</sup>Sensor is 0 for velocity and 1 for acceleration.

<sup>††</sup>ARC is 0 for back arc and 1 for along arc.

<sup>‡‡</sup>SOIL is 1 for soil site; SSOIL is 1 for soft soil (SOIL = 0, SSOIL = 0 for rock).

<sup>§§</sup>PGA is the geometric-mean horizontal peak acceleration (cm/sec<sup>2</sup>).

including a dense digital strong-motion network installed by the Institute of Engineering Seismology and Earthquake Engineering (ITSAK) in the Southern Aegean area after 2000.

After doing the analysis contained in this article we discovered that the earthquake was recorded by a broadband velocity sensor and an accelerometer in Patras, Greece (see the [Data and Resources](#) section for more information) ( $R_{HYP} = 235$  km at an azimuth of  $335^\circ$  from the epicenter), and by an accelerometer in Canukkale, Turkey ( $R_{HYP} = 523$  km at an azimuth of  $32^\circ$ ). As we had data in the azimuth

and distance ranges of these additional data, we decided that the new data would have only a minor effect on our conclusions, and thus we did not redo our analysis with the new data. We mention the additional data here for the benefit of those who might want to use it in future studies.

### Comparison of Ground Motions Obtained from Acceleration and Velocity Sensors

It is becoming widely recognized that the broadband velocity sensors provide excellent records of ground shaking

over a wider range of frequencies than acceleration sensors (although being prone to clipping for strong shaking, which generally is not a problem with our data because of the large hypocentral distances). Direct comparisons of ground motions from recordings on collocated (e.g., Paolucci *et al.*, 2008) and closely located (e.g., Jousset and Douglas, 2007) velocity- and acceleration-sensor stations show them to be virtually identical. For this kind of comparison and for further usage in our regression analysis, we converted the velocity-sensor data to acceleration time series using a standard procedure; we corrected all records for instrument response, and we removed noise effects by high-pass filtering with an acausal, second order, Butterworth filter. We chose a conservative fixed value of 0.05 Hz for the corner frequency of the high-pass filter, which we were able to do because of the high quality of the velocity-sensor dataset. Furthermore for acceleration-sensor data we followed the correction procedure described in Skarlatoudis and Margaris (2006) based on the results of Boore (2003, 2005a), with the corner frequencies of the high-pass filters being based on subjective judgment.

We made a number of comparisons of ground motions derived from velocity- and acceleration-sensor data, although we have no collocated pairs. We show in Figure 4 the FAS for two pairs of stations, separated by 3.6 and 4.8 km. The

top row of the figure is a comparison for the three components at a pair of velocity-sensor stations; the bottom row shows the comparison for a velocity-sensor station and an acceleration-sensor station (note that in this case we do not know the actual orientation of the acceleration sensor). Both comparisons suggest that the velocity-sensor data is relatively noise free to lower frequencies as compared to the acceleration-sensor data (where there seems to be a significant increase of noise in this example for frequencies less than about 2 Hz). The pair of velocity-sensor stations, which were operated by different agencies but used similar sensors with different natural frequencies (0.01 and 0.033 Hz), are in close agreement (the displacement time series for the two stations are plotted in Fig. 5). The agreement decreases somewhat as frequency increases, which could be due to spatial variation in the site response (e.g., Goda and Hong, 2008). One thing to note in all spectra in Figure 4 is the local bump in the spectrum around 0.15–0.3 Hz. As we will see, this feature is on enough recordings that it leads to enhanced motion in this frequency range in the regression fits, and an approximation of the source spectrum obtained by evaluating the regression equations at a small distance therefore shows an increase around 0.2 Hz. The comparisons in Figure 4 (and others not shown) give us confidence in combining the velocity-sensor data and the acceleration-sensor data in our analysis.

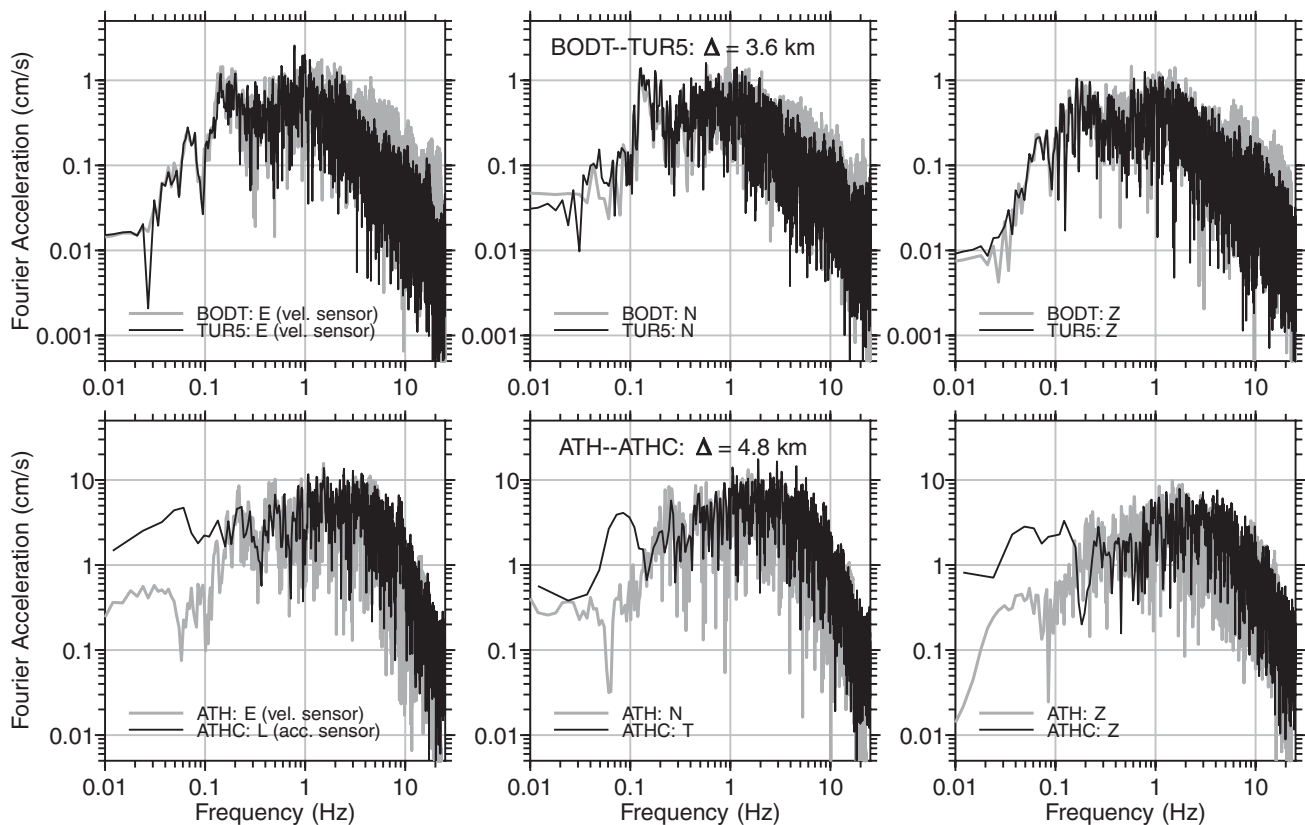


**Figure 4.** Comparison of FAS for recordings at closely located stations. The graphs show spectra from three components of motion. Top row: unfiltered records from velocity sensors; bottom row: unfiltered records from velocity sensors (ATH) and acceleration sensors (ATHC).

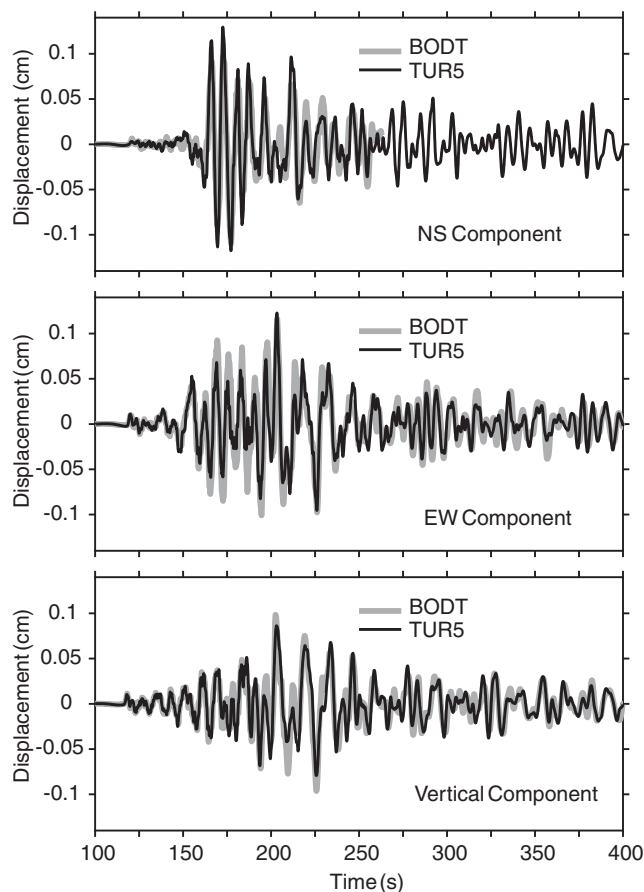


**Figure 5.** Displacement records obtained from velocity-sensor data at two closely located stations. The north–south component of BODT had a missing section of data and thus has been plotted only to the missing section (the missing section is well after the portion of strong shaking and will probably not affect the spectra computed for this component; to be cautious, however, we did not use spectra from this record in our regression analysis). Note that we shifted the BODT records to align with the TUR5 record. Also note that each component of the data was extracted independently, and therefore, the time of the first sample for each component was different. The times shown on the abscissa are relative to the first sample time of the TUR5 record for each component.

### Looking at the Data (No Regressions)

We believe that much can be gained from looking at the data, before doing any formal analysis using regression fits to functional forms. As shown in Figure 2, the recording stations span an azimuth range of about  $180^\circ$ , leaving a large gap in recordings to the west and southwest of the earthquake. On the other hand, data are available for a wide range of epicentral distances. Based on the seismotectonic properties of the broader Aegean region, as shown in Figure 1, the recording stations were divided into two groups: along-arc and back-arc stations (as shown in Fig. 2). This division was made before looking at the data from the stations.

We kept track of the high-pass filter corners used in the correction procedures for the data and only included data in the analysis for frequencies greater than 1.5 times the filter

frequency (or oscillator periods less than 0.75 the filter period, in the case of response spectra) (see Akkar and Bommer [2006] for a discussion of the relation between the usable frequency range of response spectra and filter corners). In addition, for the few stations with a low sample rate (20 samples per sec; most stations had sample rates of 100 or 200 samples per sec) we restricted the analysis to frequencies less than 8 Hz. For the FAS the upper frequency limit of the 20 samples per sec data is determined by an antialiasing filter between about 8 and 10 Hz; for the PSA we used a lower limit of 0.16 sec (6.25 Hz), based on a special simulation study of the effect of low-sampling rates on Fourier and response spectra. In this simulation we used data sampled at 200 samples per sec from stations close to those with lower sample-rate data (we studied data with both 20 and 50 samples per sec). We decimated the 200 samples per sec data to the lower sample rate and adjusted the FAS to mimic the antialiasing filter. We then computed the PSA from the resampled data and compared it to the PSA from the original data. This exercise led to the lower usable-period limit of 0.16 sec for the 20 samples per sec data, but it also showed that there is in effect no lower limit for the 50 samples per sec data—the reason being that natural processes have eliminated the higher-frequency content from the ground motion (and thus computations of the PSA at short periods are controlled by ground motions with frequencies less than those affected by the antialiasing filter). We computed whole-record FAS at 20 frequencies equally spaced logarithmically, and we smoothed the spectra using the Konno and Ohmachi (1998) smoothing filter (which smooths over logarithmically spaced frequencies). Our smoothing filter had a frequency width of 0.4 of a decade.

We plot the geometric mean of the horizontal-component FAS data in Figure 6, with each graph corresponding to a single frequency. Different symbols and colors are used for along-arc and back-arc stations and for different site classes in Figure 6. Sites were grouped into rock sites, soil sites, and soft-soil sites, based on our previous work regarding site-dependent amplification functions for the different sites in Greece (Margaris and Boore, 1998; Klimis *et al.*, 1999). Skarlatoudis *et al.* (2003) classified the local site conditions of the accelerographic stations in Greece using the same categorization proposed by the National Earthquake Hazards Reduction Program (NEHRP) (1984) and the Uniform Building Code (1997) into five discrete classes. The present classification was carried out by using the available geotechnical information for some stations while for the rest of them information from geological maps was utilized. Unlike in most, if not all, studies of strong-motion data (e.g., the appendix in Boore and Atkinson [2008], as well as the summaries by Douglas [2004, 2006, 2008]), most of the data in this study are from rock sites rather than soft-soil sites. The reason for the predominance of rock sites is that the majority of our data are from velocity-sensor stations, and these were sited on rock when possible.

There are many things to note in Figure 6. The first is the very low values of the FAS at five stations. The low values are

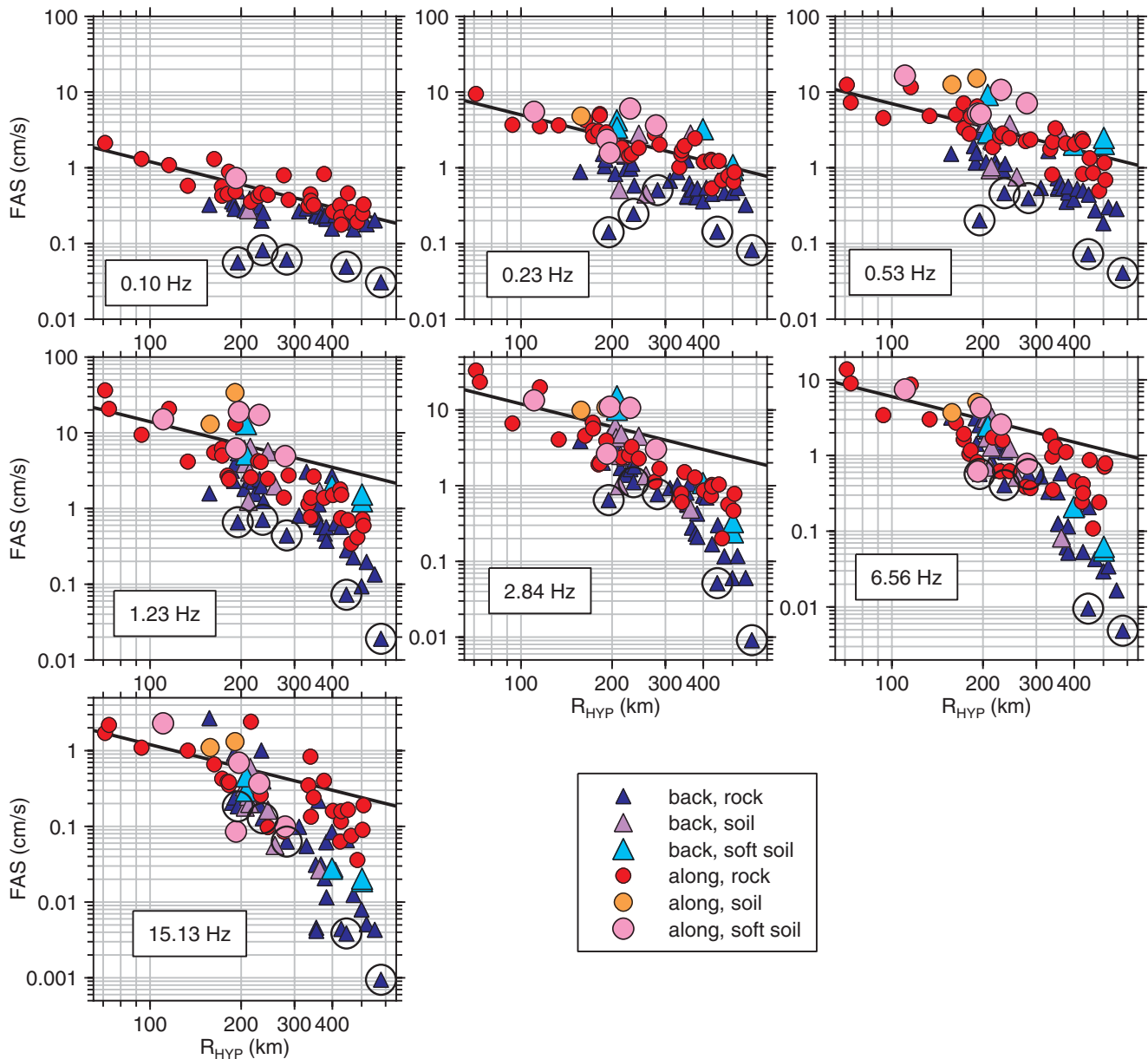


**Figure 6.** FAS versus hypocentral distance for seven log-spaced frequencies. The spectra have been smoothed over logarithmically spaced frequency intervals with width of 0.4 log units. The y axis spans the same range for all plots. The region (along and back arc) and the site conditions are indicated by the shape and color of the symbols. The five stations with unusually low amplitudes (IOSI, LIA, LKR, MYKO, and NVR) are indicated with circles enclosing the data points. The black line has a slope of  $-1$  (corresponding to a geometrical spreading of  $1/R$ ) and has been placed on the graphs by eye; it is included as a convenience to judge the relative attenuation of motions at various frequencies.

particularly obvious at low frequencies, but they persist at some stations for all frequencies. We have indicated the low-value stations in Figure 2, from which it is obvious that they are not along a single azimuth from the source, which rules out radiation pattern as an explanation of the low values. We also checked and rejected the possibility that the values happen to be low because they occur near troughs in plots of FAS versus frequency. One obvious check is to compare the motions with those from nearby stations, but unfortunately the closest stations are generally more than 30 km away, except for two cases in which the data from

the closest station are available only as a figure in Konstantinou *et al.* (2006) or from 1 Hz velocity sensors. What about site response as an explanation for the low motions? The fact that the effect is seen for very long periods (10 sec) would seem to rule out site-response. We have checked the instrument correction procedures and the filter corner frequencies and found nothing amiss; the low motions were obtained from two different instruments (STS-2 and CMG-40T/30), and the only records obtained on these instruments are for the stations with low values. In view of this, and because we cannot think of physical reasons for the low values (other

than some very strange wave-propagation effects), we conclude that the problem is instrumental or that the instrument parameters provided to us were incorrect. Fortunately these particular recordings have little impact on our conclusions; we have done the regression analyses reported in this article with and without these stations and generally find similar results (probably because most of the data are not obviously anomalous). We have excluded the data from the five stations indicated in Figure 2 from all regression analyses shown in this article.

The next thing to notice is the different distance-decay rates for the along-arc and the back-arc stations. For the lower-frequency motions it looks as if the back-arc motions are simply lower than the along-arc stations, but there is a suggestion from the higher-frequency FAS that the motions are similar to distances up to about 200 km, beyond which they diverge. The functional form that we use in our regression analysis assumes that the motions are similar near the source and diverge with increasing distance.

The motions clearly show more distance decay at high frequencies than at low frequencies. In fact, for the lowest frequencies, regression analysis finds that the motions decay somewhat less rapidly than  $1/R$ , particularly for data from back-arc stations; this led us to use a bilinear geometrical-spreading function, as discussed in a later section.

Variations of the motions for the different site classes are clearly recognizable in Figure 6, although the data are somewhat limited. In particular, the soft-soil motions are much larger than the rock motions, particularly for frequencies between about 0.2 and 3 Hz. Our site-response analysis is limited to computing the average difference of soil and soft-soil sites relative to rock sites, although there will be station-specific site responses that will not be described accurately by the overall site-response results. One such response is shown in Figure 7, which compares the FAS for two closely-spaced stations in the island of Crete: there is a factor of 5 difference in the FAS for frequencies near 0.8 Hz although the site with the higher motions is classified as a soil site, whereas the site with the lower motions is classified as a soft-soil site. We hope that by using data from many sites the central limit theorem will come to our rescue and will result in site-response estimates that are not strongly influenced by individual anomalies.

### Regression Analysis of FAS

We conclude from Figure 6 that any functional form used in a regression analysis needs to allow for three things: (1) differences between along- and back-arc motions that increase with distance, (2) curvature of the decay with distance when plotted on log-log axes, and (3) site effects. We tried regressions with various functional forms that were based on point-source geometrical spreading and anelastic attenuation. When using a single geometrical-spreading factor with an exponent of  $-1$  (so that the spreading function equaled  $1/R$ ), the anelastic coefficient at low frequencies

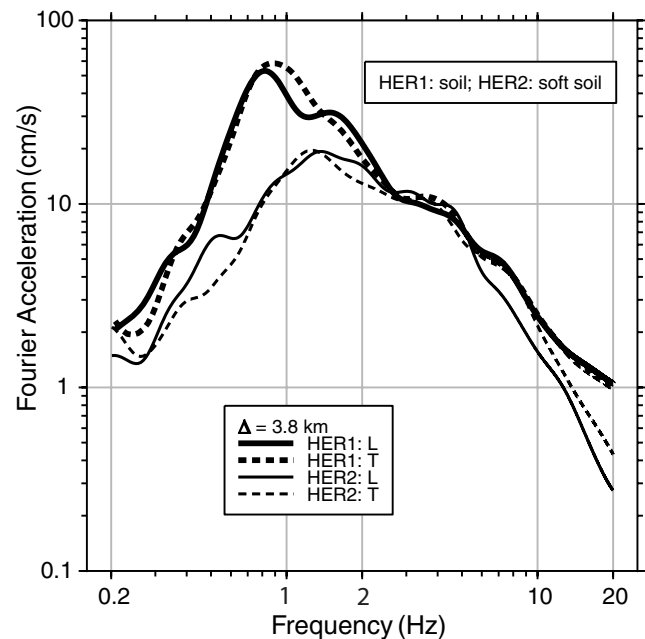


**Figure 7.** Smoothed FAS from two sites on the island of Crete separated by 3.8 km. The HER1 and HER2 sites are classified as soil and soft-soil sites, respectively.

was positive, corresponding to a positive curvature of the decay of the motion with distance. This could be avoided by using a function with a smaller exponent, such as  $1/R^{0.7}$ , but this seemed to violate the behavior of the data at closer distances (see the lines in Fig. 6). It is also clear from Figure 6 that the problem with  $1/R$  only occurs for the lowest frequencies. For higher frequencies we could use  $1/R$ , but we want a frequency-independent geometrical spreading for purposes of simulations, as assumed in a number of computer codes (e.g., SMSIM of Boore, 2005b). For this reason we prefer a bilinear geometrical-spreading model (when plotted on log-log axes). We chose the following functional form:

$$\begin{aligned} \log \text{FAS} = & c_1 + c_{21}[\log(R/R_{\text{REF}}) - H(R - R_0) \log(R/R_0)] \\ & + c_{22}H(R - R_0) \log(R/R_0) \\ & + c_{31}(1 - \text{ARC})(R - R_{\text{REF}}) \\ & + c_{32}\text{ARC}(R - R_{\text{REF}}) + c_{41}S_1 + c_{42}S_2, \quad (1) \end{aligned}$$

where the logarithms are base 10, and  $R$  is the hypocentral distance (we know of no inversions to obtain an approximation of the rupture surface from which we could obtain distance to the rupture; on the other hand, given the expected size of a rupture for a 6.7 earthquake and the large hypocentral distances, we doubt that using closest distance to the rupture would lead to any significant differences in our results). The Heaviside function  $H$  in equation (1) is defined as

$$H(\xi) = \begin{cases} 0 & \xi < 0, \\ 1 & \xi \geq 0, \end{cases}$$

ARC = 0, 1 for back-arc and along-arc stations, respectively, and  $S_1 = 1$  and  $S_2 = 1$  for soil and soft-soil sites, respectively (and 0 otherwise). Note that this functional form differs from the way that [Macias \*et al.\* \(2008\)](#) allow for along-arc and back-arc differences: they use distance-independent dummy variables (in effect, they treat the differences as they would site factors), whereas we assume that the along-arc, back-arc difference disappears for  $R_{\text{REF}}$ , with  $R_{\text{REF}} = 1$  km, which corresponds to extrapolation of motion back to the source.

Our parameterization of the site response into soil and soft-soil response relative to rock is similar to that commonly used for many years in analysis of strong motion when generic site response rather than site-specific site response is the quantity of interest. As such our parameterization will be familiar to those using our equations to estimate ground motions for practical applications. An important justification for our simple site classification into rock, soil, and soft soil is the lack of detailed site properties, including shear-wave velocity, at the majority of the recording sites.

We include the reference distance  $R_{\text{REF}}$  in equation (1) for several reasons: (1) it makes the equations dimensionally consistent with a point-source model having  $1/R$  geometrical spreading, and (2) the coefficient  $c_1$  is then the spectrum for rock motions when  $R = R_{\text{REF}}$  as the rest of the terms are equal to 0. We chose  $R_{\text{REF}} = 1$  km. (An important note is needed here: it is tempting to call the spectrum at  $R_{\text{REF}} =$

1 km the source spectrum, but it is not really the average spectrum near the source as the spectrum based on the surface observations also includes crustal amplifications and near-surface attenuation [what is generally captured in models by the parameter  $\kappa_0$ , even for rock sites]. Instead, we refer to it as a reference spectrum; comparisons, such as we show later, of the observed reference spectrum and theoretical spectra must include crustal amplifications and  $\kappa_0$  in the theoretical spectra.)

We fit the observed FAS by the aforementioned functional form using standard least-squares regression methods; Table 3 gives the coefficients for our preferred model. We then derived  $Q$  from the anelastic coefficients  $c_{31}$  (back-arc) and  $c_{32}$  (along-arc) using the equation

$$Q = -\pi f \log[\exp(1)] / (c_3 V_S), \quad (2)$$

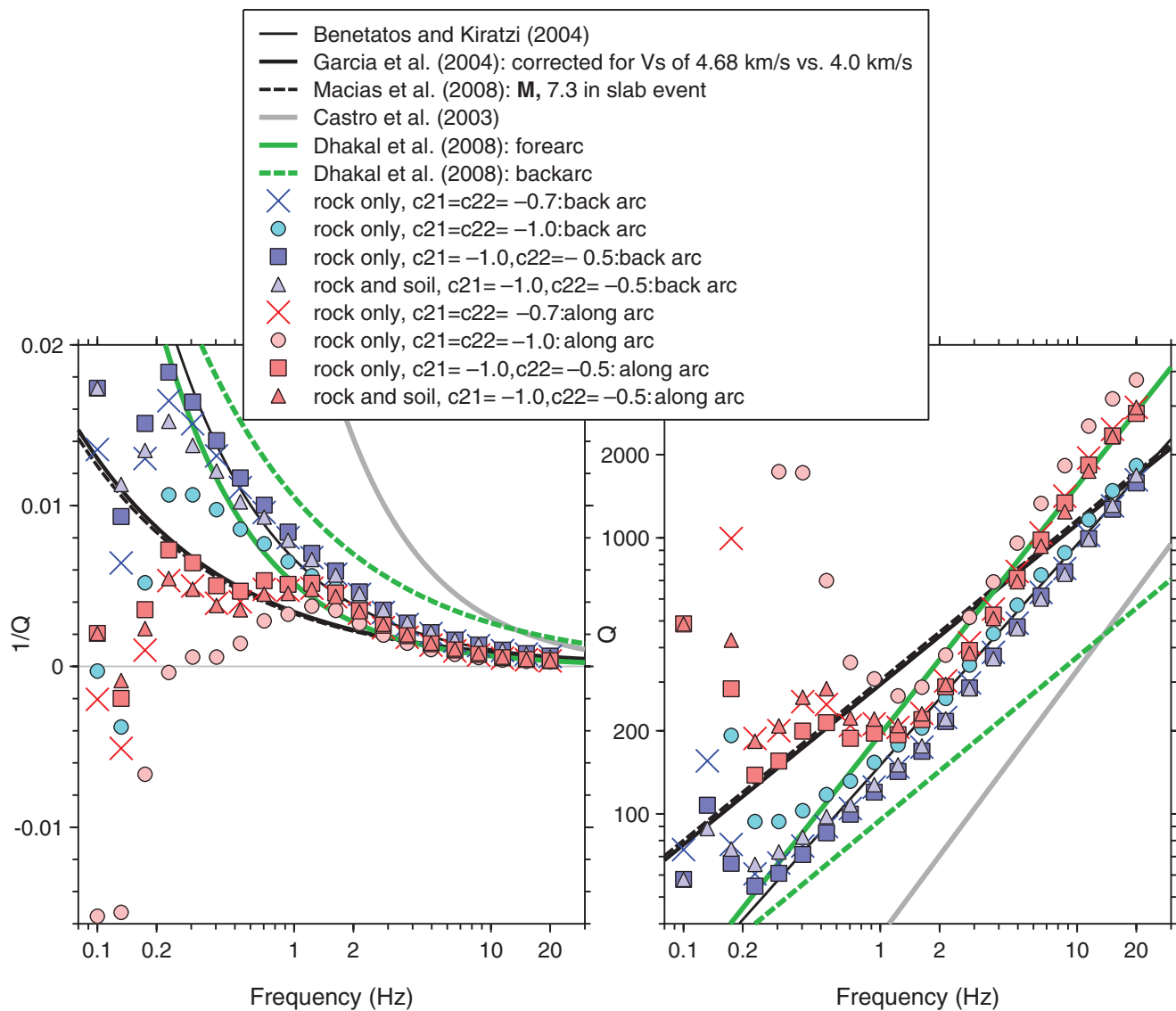
where we have suppressed the along-arc, back-arc index of  $c_3$ . We used a shear-wave velocity of 4.0 km/sec, which is close to the time-averaged velocity from the hypocenter (for which the shear-wave velocity is 4.5 km/sec) to the surface (for which the average rock velocity may be near 1.0 km/sec), for several 1D velocity models in the source area and southern Aegean area. These 1D models were extracted from a 3D velocity structure for the Hellenic area derived by a nonlinear inversion of travel times by C. Papazachos (see also [Papazachos and Nolet, 1997](#)); we used the program Vel2, written by C. Papazachos, to obtain the 1D velocity model. Figure 8 shows the results for a number of different assumptions regarding what geometrical function to

Table 3

Regression Coefficients for FAS, Produced from Both Rock and Soil Data, Excluding the Five Low Amplitude Stations

Frequency	Period	$c_1$	$c_{31}$	$c_{32}$	$c_{41}$	$c_{42}$	$\sigma_{\log \text{FAS}}$	$N_{\text{OBS}}$
0.100	10.000	2.0023	-0.00059	-0.00007	-0.428	-0.001	0.129	61
0.132	7.564	2.2225	-0.00042	0.00009	-0.124	0.094	0.130	62
0.175	5.724	2.5671	-0.00090	-0.00021	0.003	0.223	0.114	65
0.231	4.333	2.7614	-0.00144	-0.00057	0.099	0.341	0.165	66
0.305	3.278	2.7933	-0.00171	-0.00067	0.102	0.473	0.162	66
0.403	2.480	2.8646	-0.00193	-0.00069	0.183	0.551	0.176	66
0.533	1.877	2.9586	-0.00213	-0.00085	0.256	0.561	0.173	67
0.704	1.420	3.0639	-0.00241	-0.00128	0.294	0.545	0.193	67
0.931	1.074	3.1962	-0.00265	-0.00162	0.326	0.581	0.216	67
1.230	0.813	3.3274	-0.00295	-0.00217	0.300	0.535	0.220	67
1.626	0.615	3.3949	-0.00329	-0.00253	0.316	0.536	0.193	67
2.148	0.466	3.3723	-0.00339	-0.00254	0.245	0.476	0.195	67
2.840	0.352	3.3329	-0.00339	-0.00248	0.223	0.405	0.199	66
3.753	0.266	3.2574	-0.00344	-0.00244	0.237	0.345	0.220	67
4.960	0.202	3.1632	-0.00356	-0.00237	0.216	0.253	0.251	67
6.556	0.153	3.0189	-0.00364	-0.00228	0.194	0.148	0.276	67
8.664	0.115	2.9120	-0.00393	-0.00221	0.160	0.076	0.289	60
11.450	0.087	2.7016	-0.00394	-0.00213	0.083	0.042	0.339	60
15.133	0.066	2.4825	-0.00407	-0.00221	0.073	0.015	0.380	60
20.000	0.050	2.2354	-0.00432	-0.00242	0.109	0.141	0.426	60

The coefficients  $c_{21}$ ,  $c_{22}$ ,  $R_{\text{REF}}$ , and  $R_0$  have fixed values of -1.0, -0.5, 1.0, and 200, respectively, and therefore were not included as columns in the table. Soil coefficients were produced by averaging residuals (see text).



**Figure 8.**  $1/Q$  and  $Q$  derived from regression fits to the FAS. The symbols show the results using various assumptions about data included and functional form (see text). The lines show  $1/Q$  and  $Q$  as a function of frequency determined for in-slab earthquakes in other regions (Japan, [Dhakal et al. \[2008\]](#) and inferred from fig. 8 in [Macias et al. \[2008\]](#); Mexico, [García et al. \[2004\]](#); Lesser Antilles, [Castro et al. \[2003\]](#)), as well as the function determined from intermediate-depth earthquakes in the Aegean region (an average of results by [Kovachev et al. \[1991\]](#) and [Hatzidimitriou \[1995\]](#), as given in [Benetatos and Kiratzi \[2004\]](#)). [Benetatos and Kiratzi \(2004\)](#), [Dhakal et al. \(2008\)](#), [Hatzidimitriou \(1995\)](#), [García et al. \(2004\)](#), and [Macias et al. \(2008\)](#) assumed  $1/R$  geometrical spreading; [Kovachev et al. \(1991\)](#) computed the spreading for a crustal model. The [Castro et al. \(2003\)](#)  $Q$  is taken from their figure 13 for earthquakes from 72 to 130 km depth, for which the geometrical-spreading function is approximately  $1/R^{0.9}$ .

use as specified by the coefficients  $c_{21}$ ,  $c_{22}$ , and  $R_0$ ; for the bilinear function (for which  $c_{21}$  and  $c_{22}$  are not equal), we assumed  $R_0 = 200$  km, based on the data plots in Figure 6; to obtain a single geometric-spreading function we let  $c_{21}$  and  $c_{22}$  be equal to one another. We plot both  $1/Q$  and  $Q$  in the figure to show better the results at low and high frequencies. For comparison we also show some  $Q(f)$  functions taken from the literature; strictly speaking, these functions should only be compared with observed  $Q(f)$  for which the geometrical-spreading function was the same as used in the  $Q(f)$  functions taken from the literature. The

functions shown are largely based on  $1/R$  spreading, as noted in the figure caption. Our back-arc attenuation is close to that proposed by [Benetatos and Kiratzi \(2004\)](#) for intermediate-depth earthquakes in Greece for frequencies above about 0.7 Hz, whereas the  $Q$  values from intermediate-depth earthquakes in Japan and Mexico, which are remarkably similar, are in rough agreement with our along-arc attenuation derived using  $1/R$  spreading between about 0.7 and 5 Hz. Our along-arc results are in good agreement with those of [Dhakal et al. \(2008\)](#) in northern Japan above about 1 Hz. It should be noted that [Dhakal et al.](#) divide each

source-to-station path into fore-arc and back-arc mantle wedge components and solve for the  $Q$  for each portion. Thus what they call “fore-arc” and “back-arc” do not exactly coincide with our along-arc and back-arc classifications. This may explain why their back-arc  $Q$  is much lower than our back-arc  $Q$ : their back-arc  $Q$  may be strongly controlled by the attenuation within the low- $Q$  portion of the mantle, whereas ours averages over low- and high- $Q$  portions along the propagation path. Another article of interest for Japan is that of Nakamura and Uetake (2000), who used a tomographic inversion to obtain a frequency-dependent 3D distribution of  $Q$  beneath Japan and the surrounding region. The distribution of  $Q$  is similar to that in the Aegean region in that there is low  $Q$  in the mantle wedge above the subducting plate and higher  $Q$  in the subducting plate; the frequency dependence of  $Q$  in the 30–60 km layer is similar to that of Benetatos and Kiratzi (2004).

The most obvious result in Figure 8 is the difference in  $Q$  for the along-arc and the back-arc data, with the  $Q$  from the latter being smaller than the former. The lower  $Q$ s for back-arc data are needed to capture the trend of smaller motions with increasing distances as seen in Figure 6. In addition to the differences in absolute values of  $Q$ , the trends of  $Q$  versus  $f$  for the along-arc and the back-arc data diverge from one another for frequencies less than about 1 Hz. The strongest departure from the frequency trend at low frequencies is for the along-arc data. In studying the  $Q$  results in Figure 8, it is useful also to look at a graph of the standard deviation of the residuals about the various regressions, as shown in Figure 9. From Figures 8 and 9 it can be seen that including

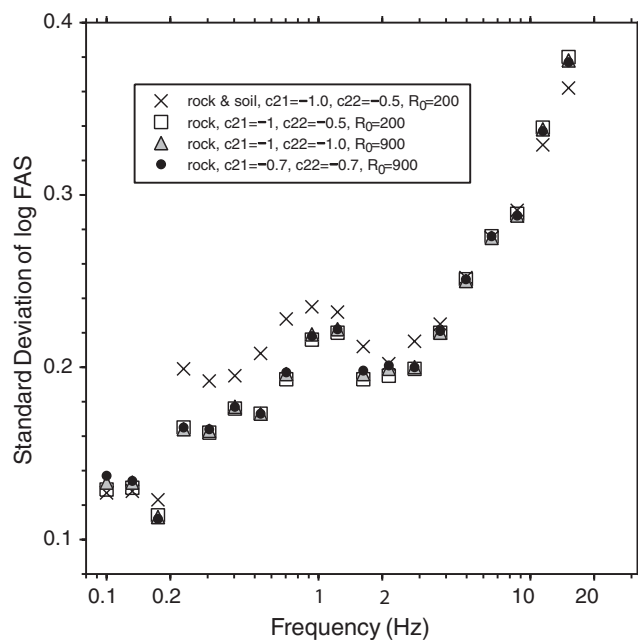


**Figure 9.** The standard deviation of the data about the regression fit using different exclusion criteria and functional forms (see text).

both rock and soil data leads to similar  $Q$  values as derived using a rock-only dataset, but that the standard deviation of the fit decreases for the rock-only dataset. On the other hand, we see that the various geometrical-spreading assumptions lead to similar values of the standard deviations but to noticeably different values of  $Q$ . In other words, the data are equally well fit using different assumed geometrical-spreading functions, but there is a correlation between the geometrical spreading and the anelastic coefficients. This correlation is well known in regression analyses of strong-motion data and means that comparisons of  $Q(f)$  alone can only be done if the geometrical spreading is the same, as mentioned previously. There is more sensitivity of  $Q$  to the geometrical-functional forms for low  $f$ , but note that the data plots in Figure 6 and the standard-deviation plots in Figure 9 show small variability in the data for low frequencies. This apparent inconsistency is explained by the fact that the low-frequency data decay at a rate close to that given by  $1/R$ , and therefore, the derived  $Q$  values could be positive or negative, leading to apparent sensitivity of  $Q$  at low frequencies to the particular model (this is best seen in the plot of  $1/Q$ ).

The standard deviations shown in Figure 9 are larger when soil coefficients are included in the regression than they are for rock-only regressions, for frequencies below about 3 Hz. This may be a reflection of the type of site-specific amplification shown in Figure 7. One interesting feature of the standard deviations in Figure 9 is that they show a general increase with frequency (this trend was also found in a recent study by Cauzzi and Faccioli [2008]). This trend is opposite to the trend often found in empirical regression analysis of response spectra from datasets that include many earthquakes (e.g., Abrahamson *et al.*, 2008).

Both the along-arc and the back-arc attenuation are expected to be influenced by wave-propagation effects in the laterally heterogeneous crust and upper mantle structure. In particular, we expect the back-arc motions to exhibit greater attenuation than the along-arc motions because of propagation through the low- $Q$  (low- $V_S$ ) mantle wedge in the back-arc direction. This effect should be more pronounced at high frequencies than low frequencies. We show in Figure 10 the ratio of back-arc to along-arc motions as a function of frequency for various hypocentral distances. Although there are complications in the ratios for frequencies less than about 1 Hz (perhaps due to wave-propagation effects in the subducting slab for the along-arc motions), in general the curves in Figure 10 agree qualitatively with our expectation.

We computed site coefficients  $c_{41}$  and  $c_{42}$  (the coefficients for soil and soft-soil sites, respectively, relative to rock sites) in two ways: by including them in the regression equations as applied to a dataset containing all types of sites and by finding the mean of the residuals of soil and rock data, where the residuals were computed as  $\log \text{FAS}(\text{observed}) - \log \text{FAS}(\text{predicted})$  and  $\log \text{FAS}(\text{predicted})$  was from a regression of the rock-only dataset. Except at the lowest frequencies, the results from both methods were similar.

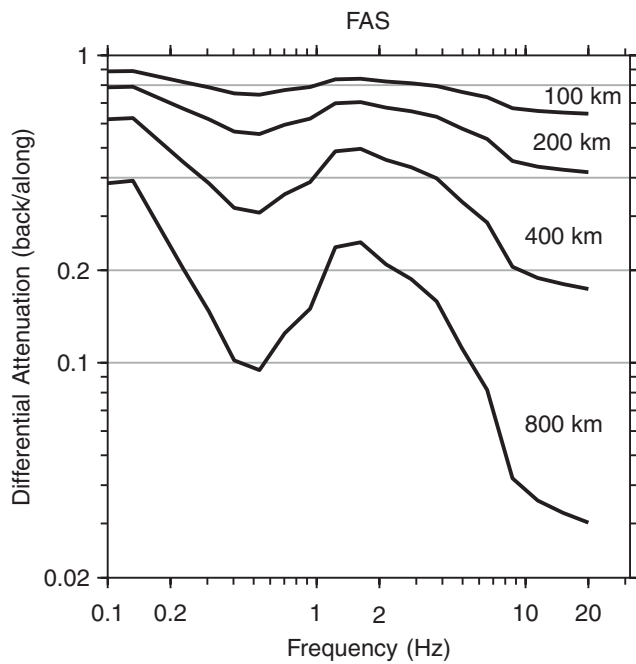


**Figure 10.** Ratio of back-arc and along-arc motions for selected distances as a function of frequency. The ratio is given by  $10^{(c_{31}-c_{32})}$ .

We converted the site coefficients to amplification (equal to  $10^{c_{41}}$  and  $10^{c_{42}}$ ). These are shown in Figure 11. Note that the amplifications approach unity at low and high frequencies. This might be expected from the physics of wave propagation: at low frequencies the wavelengths will see through the near-surface sediments and at high frequencies attenuation will tend to counterbalance the amplification for the softer sediments.

Having obtained equations giving FAS as a function of distance, we show in Figure 12 the values obtained from the equations at  $R = R_{REF} = 1$  km. We refer to these as reference spectra as they include any crustal amplifications and high-frequency attenuation (as usually parameterized by the filter  $\exp(-\pi\kappa_0 f)$ ). We show reference spectra from the equations assuming different geometrical-spreading functions and inclusion criteria. The results are similar for all geometrical-spreading functions that go as  $1/R$  out to at least 200 km, whereas the reference spectrum for the  $1/R^{0.7}$  geometrical spreading is much lower, even though the observations are fit by this spreading factor at least as well, if not better, than the other spreading functions (see the standard deviations in Fig. 9). The low values are expected because we are extrapolating the observed motions back to 1 km using a less-rapid decay than for the other results shown in Figure 12. Is there any way of deciding between the two geometrical-spreading functions? The closest data seem to be consistent with the  $1/R$  spreading (Fig. 6). There is another check: compare the reference spectra with theoretical spectra for the known moment magnitude of the earthquake. We include the source spectrum from several

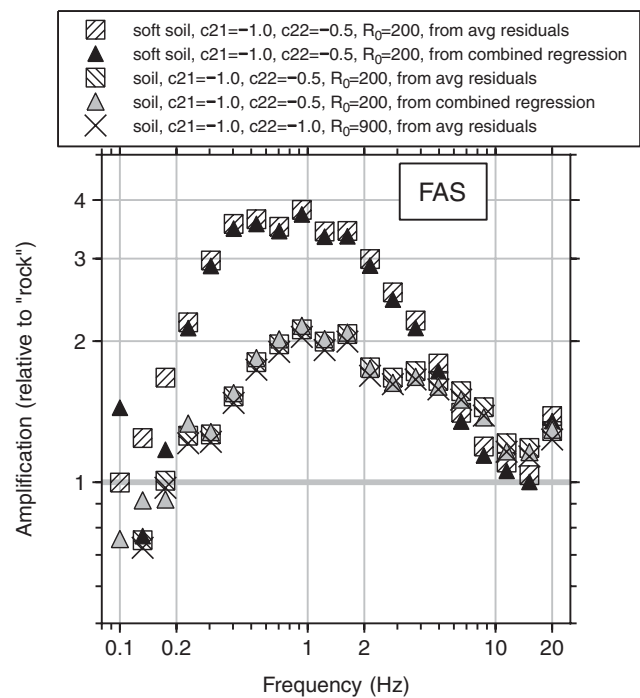


**Figure 11.** Site amplifications for FAS, relative to site class 0 (rock) site coefficients determined from rock-only regressions, for which the site coefficients are determined using the mean of the residuals and from regressions with data from all site classes, in which the soil coefficients  $c_{41}$  and  $c_{42}$  are included in the regression equations. For all but one case the two-part geometrical spreading was  $1/R$  for hypocentral distances less than 200 km and  $1/R^{0.5}$  beyond 200 km. The one exception assumed  $1/R$  over the entire distance range defined by the data.

models in Figure 12. In those models we have included crustal amplifications for a rock site as given by [Margaris and Boore \(1998\)](#) after adjusting them for the difference in density (2.7 gm/cc) and shear-wave velocity (3.4 km/sec) used by Margaris and Boore at depths of around 8 km (for which the rock amplifications were defined) and the 66 km depth of the Kythera earthquake for which we used a density of 3.24 gm/cc and a shear-wave velocity of 4.48 km/sec (from C. Papazachos' Vel2 computer program). The adjustment was simply a multiplicative factor of 1.26, given by the square root of the seismic impedances at 66 km and around 8 km. We adjusted  $\kappa_0$  and  $\Delta\sigma$  so that the model spectra agree roughly with the reference spectrum inferred from the data. As shown in Figure 12, these values are  $\kappa_0 = 0.055$  sec and  $\Delta\sigma$  between about 400 and 600 bar (this is an approximate rather than an exact range); we note that these values are high compared with values from crustal, shallow earthquakes in Greece (e.g., 56 bar found by [Margaris and Boore \[1998\]](#)) and other regions (e.g., values from California data derived by [Boore et al. \[1992\]](#) are close to 0.035 sec and 70 bar). The high value of  $\Delta\sigma$  for the Kythera earthquake is consistent with values from intraplate, intermediate-depth earthquakes in northeastern Japan ([Satoh, 2006](#)), including 1035 bar for a

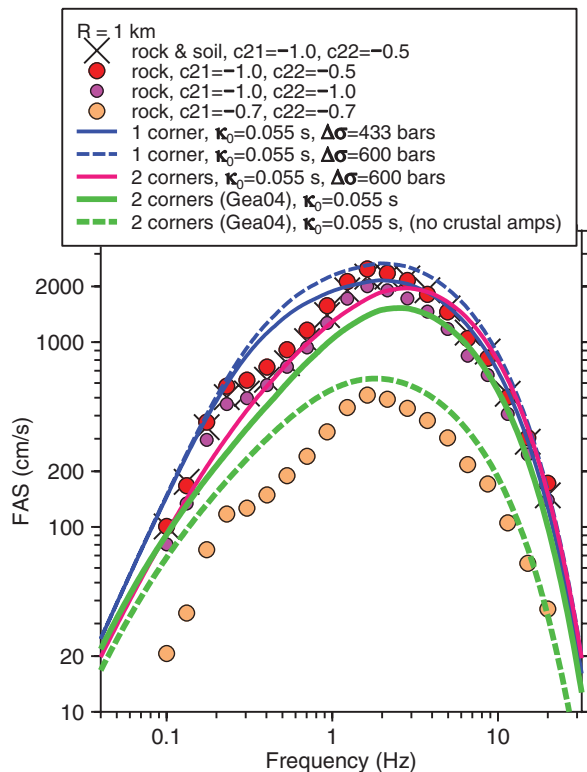


**Figure 12.** Reference FAS obtained by evaluating the regression equations at  $R = 1$  km. Results for several regressions with a variety of functional forms are shown ( $R_0 = 200$  km for all runs; the standard error of the mean is approximately equal to the size of the largest dots). The empirically determined spectra are overlaid with theoretical spectra for different source models and a constant value of the attenuation parameter  $\kappa_0$ . All models are  $\omega$ -squared models, with the acceleration being flat for frequencies sufficiently above the highest corner frequency in the absence of the  $\kappa_0$  effect. All but one model include crustal amplifications appropriate for NEHRP class B sites (see text). The “2 corners” model is a simple double-corner-frequency source model composed of a multiplication of two single-corner-frequency spectra with corner frequencies chosen to approximate the divergence of the observed spectra from a single-corner-frequency model at 0.2 Hz and yet attain approximately the peak high-frequency amplitude; the “2 corners (Gea04)” are two-corner spectra for Mexican in-slab earthquakes (García *et al.*, 2004) with and without crustal amplifications (see text).

72 km deep, **M** 7.1 earthquake, and in Vrancea, Romania (Oth *et al.*, 2009).

The single-corner frequency model clearly overshoots the observed spectrum for frequencies from about 0.2 to 1 Hz. Figure 12 also shows a simple two-corner model that is a lower bound for the observed spectrum in this frequency range; a model could undoubtedly be found that gave a good fit to the observed spectrum by introducing enough adjustable parameters, but we simply want to show a range of possibilities. We also show in Figure 12 a model found by García *et al.* (2004) from their analysis of intermediate-depth earthquakes in Mexico. Their spectrum was derived in a similar way to ours, by extrapolating a regression fit to data observed at much greater distances to 1 km. Like us, they did

not adjust the observed amplitudes for either crustal amplifications or high-frequency attenuation. For this reason, the proper comparison with our results is the dashed green curve in Figure 12 (we adjusted their spectrum for slight differences in the density and shear-wave velocity in the vicinity of their sources to be equivalent to our source properties—we did this so that the low-frequency spectral levels would be similar). For interest, we also show in Figure 12 their spectrum after multiplying by our crustal amplifications. In either case, the motions for the Mexico earthquakes are smaller than for the Kythera earthquake. But returning to the question of the geometrical spreading out to about 200 km, the reference spectrum inferred using the  $1/R$  spreading function is consistent with the level expected for the moment magnitude of the earthquake, whereas the  $1/R^{0.7}$  spreading function is not consistent. This is the strongest evidence against the  $1/R^{0.7}$  spreading function.

### Regression Analysis of PSA

Although we have emphasized FAS in this article because parameters of use in simulating ground motions can be found directly from FAS, we fit equation (1) to 5% damped PSA; Table 4 gives the coefficients for our preferred model. The PSA equations might be more directly useful in engineering practice than FAS, although the great distances from the source to the sites means that most of the observed motions are quite low and having only one earthquake we obviously have no constraint on magnitude scaling. We show PSA data for rock sites and regression fits as a function of distance for peak ground acceleration (PGA) and oscillator periods of 0.2, 1.0, and 3.0 sec in Figure 13. The PSA are similar to the FAS data in that they show a divergence with distance between along-arc and back-arc stations, with back-arc motions being lower; also similar is the less-rapid distance decay of motions with decreasing frequency. Figure 13 also compares the Kythera response spectra to those predicted from four ground-motion prediction equations (GMPEs) based on data in other parts of the world, as discussed in the next section.

One thing to note is the high value of the motion at the two closest stations (ANS1 and KYT1) compared to our predictions. As these are the highest ground motions in the dataset, we should not summarily dismiss the high values as being merely random variation. They might be high because of a less-rapid-than-usual geometrical spreading from the source (related to wave propagation in the subducting slab), source directivity, or the finiteness of the fault (with the portion contributing to the peak motion being closer than the hypocentral distance; simulations suggest that this could increase the motions by less than a factor of 1.2). We have no answers, but merely caution that if there is a physical reason for the high values compared to our predictions, then use of our prediction equations for other sites at comparable distances might lead to ground-motion values that are too low.

Table 4  
Regression Coefficients for PSA, Produced from Both Rock and Soil Data, Excluding the Five Low Amplitude Stations

Frequency	Period	$c_1$	$c_{31}$	$c_{32}$	$c_{41}$	$c_{42}$	$\sigma_{\log PSA}$	$N_{OBS}$
PGV	PGV	2.5716	-0.00249	-0.00152	1.291	1.409	0.163	60
PGA	PGA	3.8930	-0.00383	-0.00254	0.260	0.433	0.233	60
100.000	0.010	3.8921	-0.00383	-0.00254	0.262	0.434	0.233	60
50.000	0.020	3.8936	-0.00383	-0.00255	0.275	0.443	0.234	60
33.333	0.030	3.9330	-0.00390	-0.00261	0.255	0.428	0.238	60
20.000	0.050	4.0261	-0.00409	-0.00270	0.222	0.390	0.246	60
13.333	0.075	4.1188	-0.00414	-0.00269	0.216	0.360	0.264	60
10.000	0.100	4.1832	-0.00417	-0.00259	0.239	0.348	0.271	60
6.667	0.150	4.2290	-0.00402	-0.00263	0.280	0.350	0.273	67
5.000	0.200	4.2804	-0.00398	-0.00274	0.262	0.383	0.265	67
4.000	0.250	4.2447	-0.00380	-0.00263	0.299	0.440	0.251	67
3.333	0.300	4.2439	-0.00377	-0.00271	0.283	0.473	0.239	67
2.500	0.400	4.2548	-0.00389	-0.00286	0.247	0.480	0.198	67
2.000	0.500	4.1619	-0.00372	-0.00281	0.281	0.539	0.207	67
1.333	0.750	4.0190	-0.00345	-0.00261	0.308	0.539	0.236	67
1.000	1.000	3.7742	-0.00312	-0.00201	0.352	0.642	0.227	67
0.667	1.500	3.4293	-0.00272	-0.00145	0.309	0.604	0.190	67
0.500	2.000	3.2107	-0.00248	-0.00109	0.359	0.637	0.177	67
0.333	3.000	2.8977	-0.00205	-0.00082	0.242	0.589	0.192	67
0.250	4.000	2.7467	-0.00186	-0.00087	0.231	0.488	0.209	67
0.200	5.000	2.5991	-0.00158	-0.00068	0.206	0.435	0.160	66
0.133	7.500	2.0849	-0.00101	-0.00033	0.140	0.308	0.143	62
0.100	10.000	1.8151	-0.00119	-0.00041	0.053	0.287	0.146	61

The coefficients  $c_{21}$ ,  $c_{22}$ ,  $R_{REF}$ , and  $R_0$  have fixed values of  $-1.0$ ,  $-0.5$ ,  $1.0$ , and  $200$ , respectively, and therefore were not included as columns in the table. Soil coefficients were produced by averaging residuals (see text).

We computed site amplifications just as we did for the FAS. The results are shown in Figure 14. As for the FAS amplifications in Figure 11, the method of deriving the amplification (averaging residuals of rock-only regression or including the amplifications as coefficients in the complete dataset) makes little difference in the results except at the lowest frequencies. What is interesting in the comparison of Figures 11 and 14 are the similarities and differences in the PSA and the FAS amplifications. Both amplifications peak in the range of 0.3 to 2 Hz, with similar amplitudes near the peak for FAS and for PSA. The peak of the soft-soil amplification occurs at a somewhat lower frequency than the soil amplification. But the FAS amplifications decrease more rapidly than the PSA amplifications at low and high frequency. The differences are probably a reflection of the fundamental differences in FAS and PSA: the former is a measure of the ground motion at a specified frequency, whereas the latter is a measure of the response of an oscillator with a specified frequency to a ground motion that may have no energy at the specified oscillator frequency. In particular, PSA must approach the PGA asymptotically at high oscillator frequencies, although the frequencies of ground motion controlling peak acceleration may be much lower. This makes it hard to interpret the PSA amplification in terms of a physical process acting on the ground motions. FAS amplifications give more fundamental information about the physical processes affect-

ing the ground motion, while the PSA amplifications are useful mainly for engineering purposes.

The PSA amplifications are compared to those from recent empirical analyses of ground-motion data by Choi and Stewart (2005), as modified slightly by Boore and Atkinson (2008) (which we refer to as the CS05[BA08] amplifications), in Figure 15. In making the comparison we need to choose the average shear-wave velocities for the CS05 (BA08) amplifications. We assume that the soil and soft-soil sites correspond to NEHRP class C and D sites, respectively, with average velocities of 520 and 250 m/sec (see the appendix in Boore and Atkinson, 2008). For the average velocity corresponding to rock we show the results of four choices in Figure 15: 1070, 1500, 2000, and 2500 m/sec. The first value is the geometric mean of the velocities defining an NEHRP class B rock site. We see from Figure 15 that the overall shape of the amplification versus period is similar but that the absolute values differ according to the chosen velocity for rock; the amplifications from the Kythera PSA are in better agreement with the CS05(BA08) amplifications for higher values of the reference velocity (a value near 1500 m/sec for periods longer than about 0.5 sec and near 2500 m/sec for shorter periods) than the NEHRP class B velocity. While we cannot expect an exact match between the Kythera PSA and the CS05(BA08) amplifications, the systematic mismatch for a reference velocity of 1070 m/sec may be meaningful. If so, it is saying that either the average

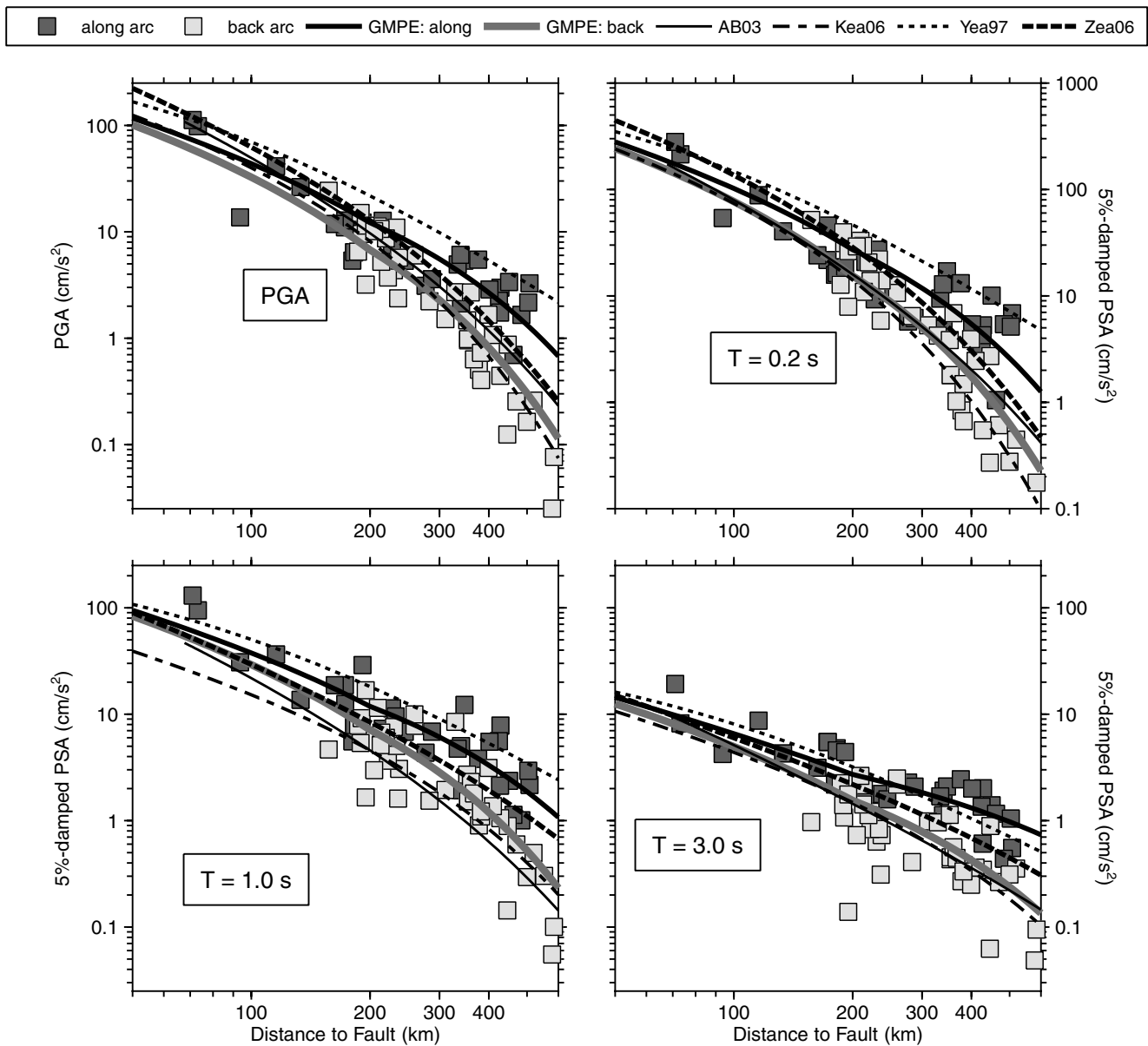


**Figure 13.** Comparison of observed 5% damped PSA for rock sites with empirical ground-motion predictions from our analysis of the data and from several published GMPEs for in-slab earthquakes based on data from other parts of the Earth (AB03, Atkinson and Boore, 2003; Kea06, Kanno *et al.*, 2006; Yea97, Youngs *et al.*, 1997; Zea06, Zhao *et al.*, 2006). The Kea06 motions do not include their correction for anomalous seismic intensity in northwestern Japan. The results are shown for PGA and three oscillator periods as a function of distance.

velocities chosen for the soil and soft-soil sites are too high or that the rock reference velocity is too low. Unfortunately, there are few actual measurements of the average velocities at the recording sites, so it is not possible to draw any definitive conclusions.

#### Comparison with Ground Motions from Other Earthquakes

It is important in estimating ground motions for engineering purposes to know if the ground shaking from the

Kythera intermediate-depth earthquake was similar to that from shallow Greek earthquakes of comparable magnitude, recorded at similar distances. If the motions are comparable, they can be added to the database of strong-motion data and used to produce GMPEs from empirical regression analysis of the complete dataset. If the motions are different, however, then this must be taken into account in estimating the earthquake hazard for intermediate-depth earthquakes in Greece. In this regard, it is then important to compare the motions with those from intermediate-depth earthquakes located elsewhere in the world (no other Greek intermediate-depth

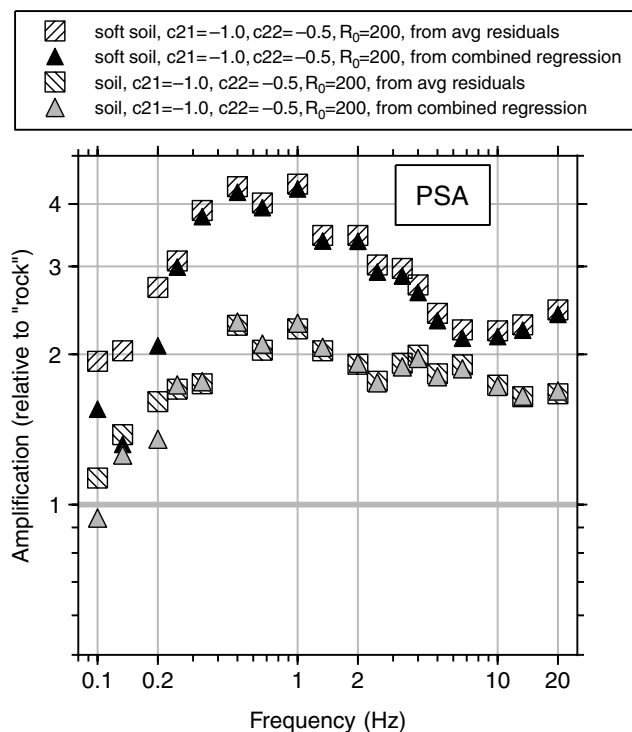


**Figure 14.** Site amplifications from PSA, relative to site class 0 (rock) site coefficients determined from rock-only regressions, for which the site coefficients are determined using the mean of the residuals and from regressions with data from all site classes, in which the soil coefficients  $c_{41}$  and  $c_{42}$  are included in the regression equations. The two-part geometrical spreading was  $1/R$  for hypocentral distances less than 200 km and  $1/R^{0.5}$  beyond 200 km.

earthquakes of magnitudes between 6.5 and 7.0 have produced a dataset of ground shaking that is at all comparable to that from the Kythera earthquake).

We studied the catalog of Greek earthquakes to find shallow events with magnitudes within 0.1 unit of Kythera's magnitude ( $M$  6.7) recorded at comparable hypocentral distances. We found two shallow events: the 1983 North Aegean Sea  $M$  6.8 event, depth = 12 km, and the 1995 Kozani-Grevena  $M$  6.6 event, depth = 3.0 km. We compare the response spectra from these recordings with the spectra from Kythera recordings in Figure 16. At first glance we might draw the important conclusion from this figure that the ground motions from the Kythera earthquake are significantly higher than those from shallow Greek earthquakes for comparable recording distances and magnitudes. This means that the motions cannot be combined with the recordings from shallow earthquakes, and thus special analysis and consideration must take place to estimate the earthquake hazard from these earthquakes both in terms of peak ground and spectral shaking. On closer examination, however, we note that the motions for the Kythera earthquake in three of the graphs are from the two closest stations—ANS1 and KYTH1—that we earlier pointed out that seem to have higher-than-average motions compared to our regression curves. In

addition, the Kythera motions in the upper right-hand graph are from a station (HAN1) located on soil; we show by the dashed curves in Figure 16 that the HAN1 PSA corrected to a rock site based on the PSA amplifications shown in an earlier figure are comparable to the shallow-earthquake spectrum. The correction to an equivalent rock site was obtained by dividing the recorded PSA by the geometric-mean amplifications for soft-soil site (as given by fitting a fourth-order polynomial to the empirical amplifications in Fig. 14). So it is not clear to us from the comparisons shown in Figure 16 that the Kythera motions are indeed larger than expected for shallow earthquakes in Greece. On the other hand, we note that the stress parameters needed to fit the extrapolated reference spectrum to a model are almost ten times higher than those inferred from recordings of shallow earthquakes in Greece (e.g., Margaris and Boore [1998] and Margaris and Hatzidimitriou [2002] find that a stress parameter close to 60 bar explains many ground motions from shallow earthquakes). This would be consistent with the ground motions from the Kythera earthquake being higher than for an average shallow earthquake in Greece.

We compare the motions from the Kythera earthquake to those from other intermediate-depth in-slab earthquakes in two ways: (1) direct comparison to a pair of well-recorded earthquakes near Taiwan, and (2) comparison to values obtained from empirically based GMPEs.

About 1 yr after the Kythera earthquake, an earthquake doublet occurred off the southern tip of Taiwan. These earthquakes were somewhat larger than the Kythera earthquake ( $M$  7.0 and 6.9), and they were at shallower depths than the Kythera earthquake (near 50 km). Like the Kythera event, however, they occurred within the subducting slab, and they were very well recorded over a limited range of azimuths (Wu *et al.*, 2008). We compare the geometric means of the 5% damped PSA from horizontal components of these two earthquakes (the Pingtung earthquakes) with the Kythera motions in Figure 17. Because the attenuation with distance might be different in the two regions, it may be best to concentrate on the motions within about 200 km. The along-arc motions for the Kythera earthquake are comparable to those from the Pingtung earthquakes (and the paths to the Pingtung recording stations may be more similar to along-arc paths than to back-arc paths, which travel out of the slab and through the asthenosphere, although the Taiwan plate geometry is more complicated than the case for the Kythera earthquake). It is well known that magnitude scaling is larger for long-period response spectra than for short periods, and therefore, we would expect less difference between the events at short periods than at long periods. But the Kythera earthquake along-arc motions and the Pingtung earthquake motions are also comparable at a 3 sec period. Does this mean that the Kythera along-arc motions are unusually large, or that larger-magnitude Pingtung earthquake motions are low? Wu *et al.* (2008) conclude that the first Pingtung earthquake has motions somewhat smaller than expected from the global dataset, whereas the motions from the second event

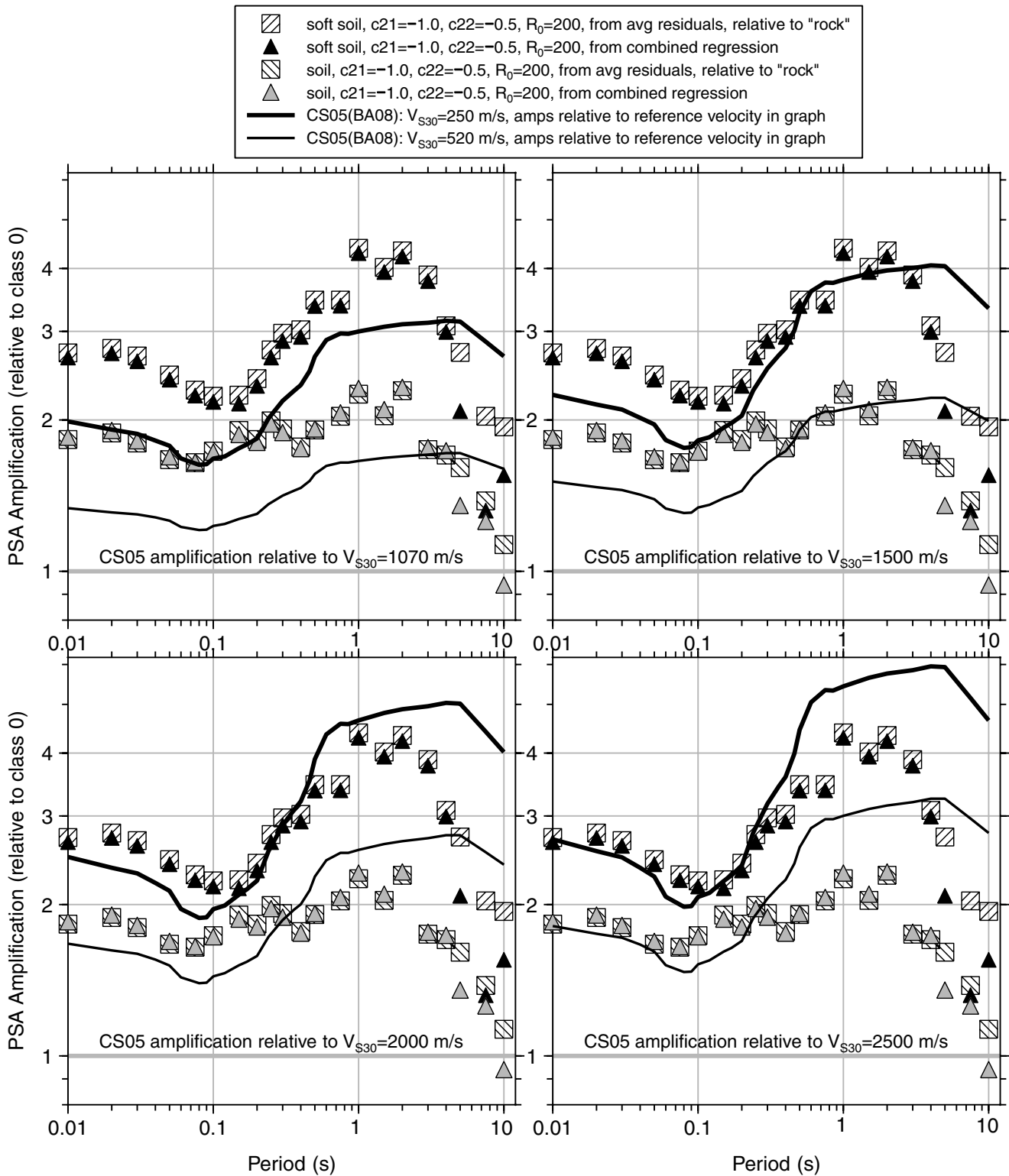


**Figure 15.** Site amplifications from PSA regressions compared to amplifications due to Choi and Stewart (2005) (CS05), as modified by Boore and Atkinson (2008) (BA08) for four values of the reference velocity and a peak rock acceleration of 0.005g.

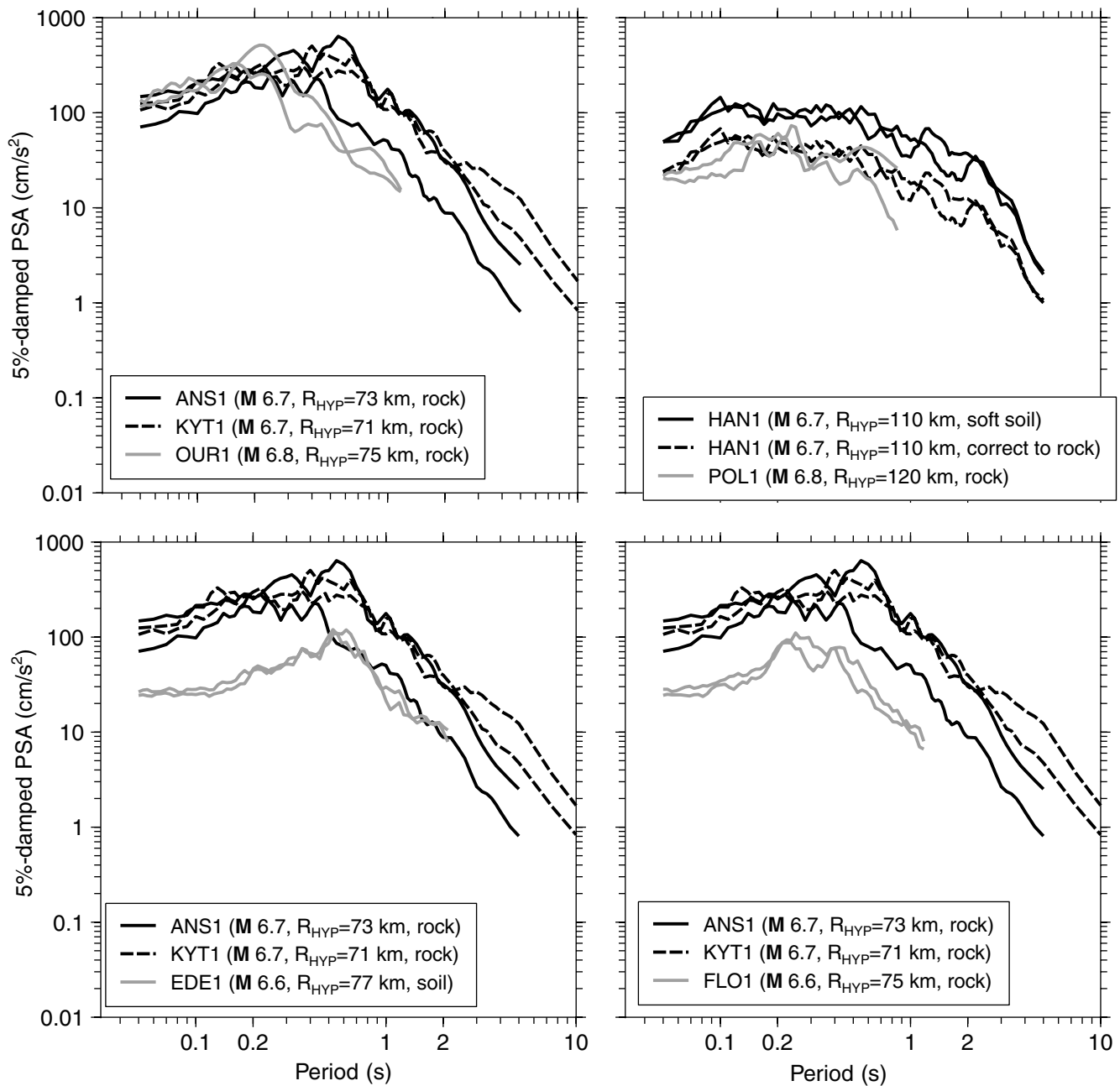


**Figure 16.** Comparison of PSA for recordings of the Kythera earthquake (black) and recordings of two shallow earthquakes with magnitudes comparable to the magnitude of the Kythera earthquake and similar hypocentral distances (gray). In the upper right-hand graph the black dashed lines are the HANI spectra reduced to an equivalent rock site (see text).

are comparable to the average motions based on the global regression analysis.

The second way of judging if the ground motions for Kythera are representative of those from other in-slab earthquakes is to compare the motions with predictions from GMPEs. Such comparisons are given in the earlier Figure 13. While there is a wide range of motions from the various GMPEs, in general the Kythera along-arc motions are larger than expected for an average in-slab earthquake. For all but the Youngs *et al.* (1997) GMPEs, the Kythera along-arc mo-

tions are higher than the predictions, whereas the back-arc motions are relatively consistent with the three other GMPEs. The Zhao *et al.* (2006) predictions are the best compromise between the along-arc and back-arc motions. To show the results of our empirical regression fit to more oscillator periods, in Figure 18 we compare our motions with those of other GMPEs as a function of period for a hypocentral distance of 250 km (the approximate center-of-mass of our data). As we found in Figure 13, the Zhao *et al.* (2006) GMPEs provide the best fit to the average of the along-arc

Class A, B, C (Lee for  $V_{S30}$ ): ○ PingTung #1 (M 7.0) + PingTung #2 (M 6.9) ■ Kythera (M 6.7), along arc □ Kythera (M 6.7), back arc

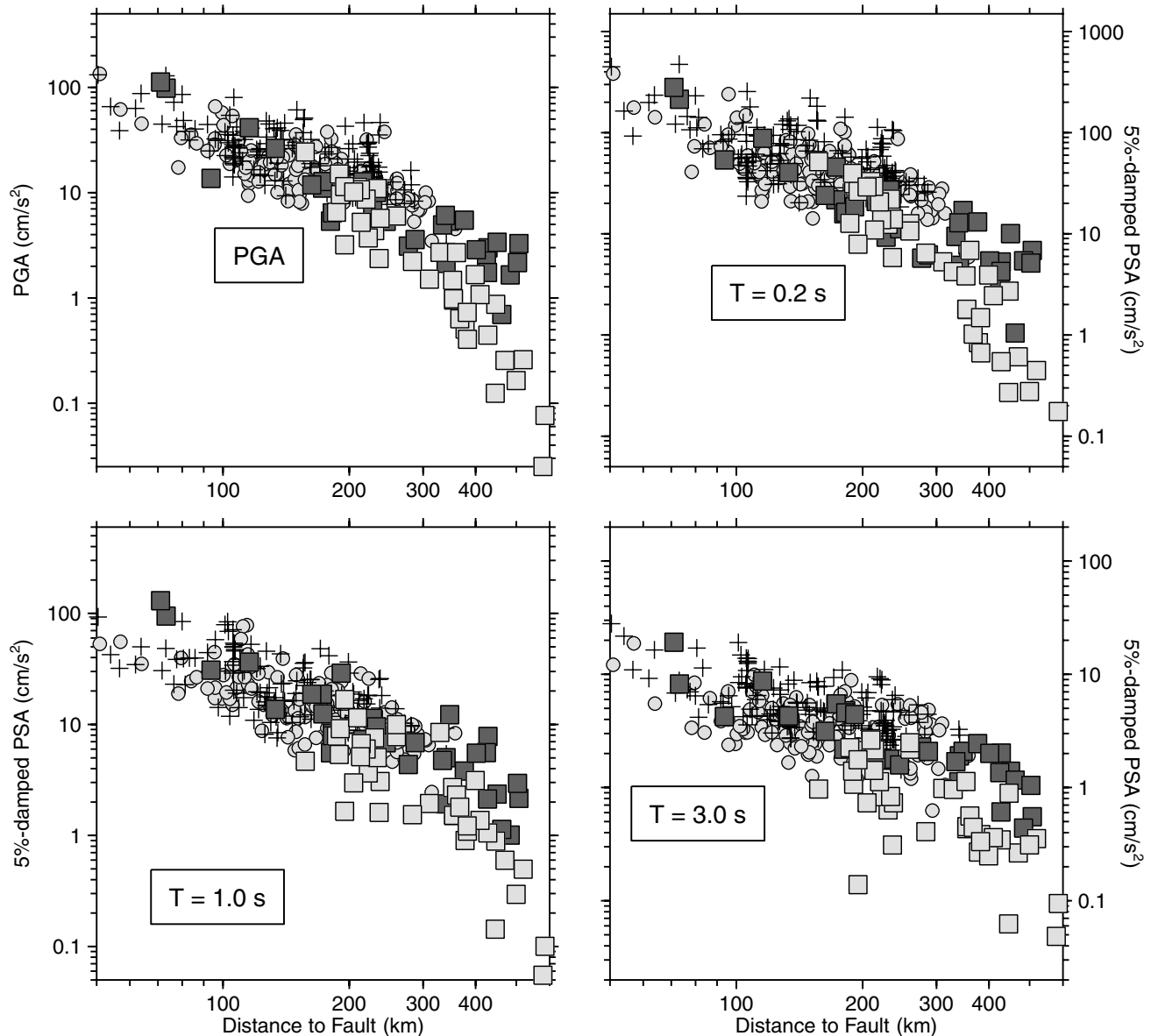


**Figure 17.** Comparison of 5% damped PSA at rock and rock-like sites for the Kythera earthquake and two earthquakes occurring south of the southern tip of Taiwan (Wu *et al.*, 2008). The two Taiwanese earthquakes, called the Pingtung earthquakes, occurred 8 min apart; they are in-slab events at depths near 50 km. Only Pingtung data from stations with  $V_{S30} > 360$  m/sec (according to Lee and Tsai, 2008) are plotted.

and back-arc motions, except at short periods, where the Atkinson and Boore (2003) are in better agreement with the observations.

### Conclusions

We collected all the available data from the M 6.7 in-slab earthquake occurring near the island of Kythera in Greece on 8 January 2006 and used them in establishing

the most complete (so far) database for an intermediate-depth earthquake in the South Aegean area. Most of the data are from broadband velocity sensors. We found good agreement between broadband velocity-sensor data and acceleration-sensor data, and thus we combined the two type of data in our analysis. We performed regression analyses on both the FAS and the PSA. A hinged bilinear geometrical-spreading function was used in the regression fit. The  $Q$  from the regression of FAS increases strongly with frequency above

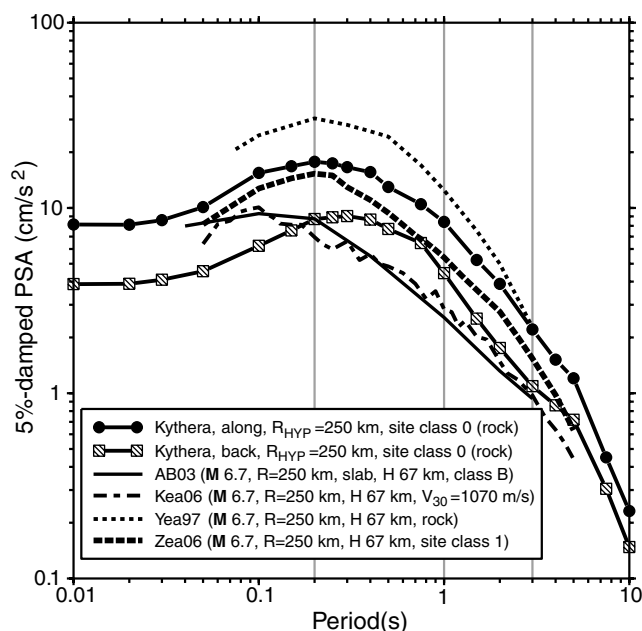


**Figure 18.** Comparison of observed 5% damped PSA for site class 0 (rock) sites with empirical ground-motion predictions from our analysis of the data and from several published GMPEs for in-slab earthquakes based on data from other parts of the Earth (AB03, Atkinson and Boore, 2003; Kea06, Kanno *et al.*, 2006; Yea97, Youngs *et al.*, 1997; Zea06, Zhao *et al.*, 2006). The results are shown at a distance of 250 km (the approximate center-of-mass of our data) as a function of the oscillator period.

about 1.5 Hz for the along-arc motions and above 0.2 for the back-arc motions. The attenuation for motions from back-arc stations is much greater than for motions from along-arc stations. This difference in attenuation leads to relatively smaller high-frequency back-arc motions with increasing distance, probably as a result of propagation through the low-velocity (low- $Q_S$ ) layer in the mantle wedge. The attenuation for the along-arc motions levels off or even decreases for frequencies less than about 1 Hz, which may be a wave-propagation effect in the subducting slab. The standard deviations of the residuals about the regressions depend little on the functional form used in the regressions. The standard deviations of log FAS increase with frequency, from about 0.11 at 0.2 Hz to 0.42 at 20 Hz, unlike the standard deviations on empirical GMPEs.

Although most of the data are from rock sites, clear site amplifications are found from the less abundant soil and soft-soil data. The amplifications from the soil-site data show greater amplifications on soft-soil sites than on soil sites. The amplifications peak between about 0.4 and 2.0 Hz, with amplifications of about 2.0 and 4.0 for soil and soft-soil sites, respectively, relative to the rock-site motions. The soft-soil amplification seems to extend to somewhat lower frequencies than the soil amplification. The FAS amplifications approach unity near 0.1 Hz and 10 Hz.

We extrapolated the motions to 1 km to form reference spectra. The reference spectra are consistent with the independently determined seismic moment when a geometrical

spreading of  $1/R$  is assumed out to 200 km; a geometrical spreading of  $1/R^{0.7}$  fits the data well but is inconsistent with the seismic moment. A single-corner frequency model with a stress parameter of about 400–600 bar fits the peak part of the spectrum, but it overestimates the observed spectrum for frequencies from about 0.2 to 1 Hz. We showed that a spectrum for a simple two-corner model forms a lower bound for the observed spectrum in this frequency range. The diminution parameter  $\kappa_0$  needs to be around 0.055 sec in order to explain the spectral decay at high frequencies; this is larger than often found for rock-site data (e.g., Boore *et al.* [1992] and Boore and Joyner [1997] find  $\kappa_0$  near 0.02 and 0.035 sec, respectively, is required to fit ground motions from western North America).

Regressions of PSA show roughly similar trends as the FAS regressions, with the back-arc PSA becoming increasingly smaller than the along-arc PSA with increasing distance. The site amplifications are also similar to the FAS amplifications in the frequency range of largest amplifications. Comparisons with empirical amplifications from an extensive database, primarily from California, show rough agreement in the period dependence of the amplifications, although the amplifications from the Kythera earthquake are systematically high. This may be due to the average velocities of 250, 520, and 1070 m/sec assumed for the soft-soil, soil, and rock stations, respectively, that recorded the Kythera earthquake. More measurements of the shear-wave velocities at the recording stations are needed to investigate the inconsistency.

Overall, the PSA are comparable to motions from intermediate-depth, in-slab earthquakes in other parts of the world, although the along-arc motions are generally higher than from predictions of motions from other in-slab earthquakes (which do not differentiate between along- and back-arc motions). Comparisons with shallow earthquakes in Greece at comparable hypocentral distances and similar magnitudes are equivocal but suggest that the Kythera motions are higher than expected from shallow earthquakes in Greece. More definitive evidence for the higher ground motions from the intermediate-depth Kythera earthquake than other shallow earthquakes in Greece comes from the stress parameter required to fit spectra from earthquakes in Greece: the stress parameter from the Kythera earthquake is about ten times higher than that found from data from shallow earthquakes.

All evidence points to the motions from the Kythera earthquake being different than other shallow earthquakes in Greece, and thus the data from the Kythera earthquake should not be mixed with the shallow-earthquake data when deriving GMPEs. This means that special analysis and consideration must take place in estimating the earthquake hazard from intermediate-depth earthquakes in Greece, although the comparison with GMPEs from other intermediate-depth earthquakes indicates that those GMPEs can be used to estimate ground motions, as long as corrections are made for the higher along-arc motions. Much development has occurred or will occur on the lands comprising

the outer arc in the southern part of the Aegean sea (from the Peloponnesus Peninsula on the west, Crete to the south, and Rhodes to the east), and thus the higher along-arc motions must be taken into account in seismic hazard estimates. We note in particular that the motions at the two closest stations, on Kythera and Crete, may be particularly high. This may be due to less-rapid-than-usual geometrical spreading from the source, to wave propagation in the subducting slab, to source directivity, or to the portions of the finite fault leading to the peak motions being closer to the stations than the hypocenter. More data or detailed modeling is required to choose between these possibilities.

### Data and Resources

Velocity-sensor data used in this study were collected using the permanent Greek seismological networks, operated by the National Observatory of Athens (NOA) and the Aristotle University of Thessaloniki, and are available to the public upon request. The main body of broadband velocity-sensor recordings for this earthquake came from the EGELADOS temporary network and cannot be released to the public. Additional broadband velocity-sensor recordings were used from the Kandilli Observatory and Earthquake Research Institute (KOERI) and GEOFON and are available from the corresponding online databases, <http://barbar.koeri.boun.edu.tr/sismo/zKDRS/login.asp> (last accessed March 2009) and <http://geofon.gfz-potsdam.de/cgi-bin/geofon//request?mode=nform&nettype=perm> (last accessed March 2009), respectively. The Web site for broadband velocity sensor and accelerometer in Patras, Greece, is <http://seis30.karlov.mff.cuni.cz> (last accessed May 2009).

Acceleration-sensor data used in this study were collected using the acceleration-sensor networks operated by the Institute of Engineering Seismology and Earthquake Engineering (ITSAK), the NOA, the Public Power Corporation, and the Astronomical Observatory of Larissa. Data from ITSAK and NOA networks are available upon request, while data from the other two acceleration-sensor networks cannot be released to the public.

### Acknowledgments

We thank Chris Stephens and Carola Di Alessandro for useful conversations and Francisco Chávez-García, John Douglas, Yoshimitsu Fukushima, and Willie Lee for helpful reviews.

We are also grateful to the National Observatory of Athens (Geodynamic Institute), the Public Power Corporation, and the Astronomical Observatory of Larissa for their contributions to the acceleration-sensor dataset of this work.

This work was partially supported by the EC Project "ITSAK-GR" Project Number MTKD-CT-2005 029627.

### References

Abrahamson, N., G. Atkinson, D. Boore, Y. Bozorgnia, K. Campbell, B. Chiou, I. M. Idriss, W. Silva, and R. Youngs (2008). Comparisons of the NGA ground-motion relations, *Earthq. Spectra* **24**, 45–66.

- Aguirre, J., and K. Irikura (2007). Source characterization of Mexican subduction earthquakes from acceleration source spectra for the prediction of strong ground motion, *Bull. Seismol. Soc. Am.* **97**, no. 6, 1960–1969.
- Akkar, S., and J. J. Bommer (2006). Influence of long-period filter cut-off on elastic spectral displacements, *Earthq. Eng. Struct. Dyn.* **35**, 1145–1165.
- Atkinson, G. M., and D. M. Boore (2003). Empirical ground-motion relations for subduction zone earthquakes and their application to Cascadia and other regions, *Bull. Seismol. Soc. Am.* **93**, 1703–1729.
- Benetatos, C. A., and A. A. Kiratzi (2004). Stochastic strong ground motion simulation of intermediate depth earthquakes: the cases of the 30 May 1990 Vrancea (Romania) and of the 22 January 2003 Karpathos island (Greece) earthquakes, *Soil Dyn. Earthq. Eng.* **24**, 1–9.
- Benetatos, C., and A. Kiratzi (2006). Source characteristics of the 8 January 2006 ( $M_w$  6.7) intermediate depth Kythera earthquake, *1st European Conference on Earthquake Engineering and Seismology (ECEES)*, 3–9 September 2006, Geneva, Switzerland.
- Boore, D. M. (2003). Analog-to-digital conversion as a source of drifts in displacements derived from digital recordings of ground acceleration, *Bull. Seismol. Soc. Am.* **93**, 2017–2024.
- Boore, D. M. (2005a). On pads and filters: Processing strong-motion data, *Bull. Seismol. Soc. Am.* **95**, 745–750.
- Boore, D. M. (2005b). SMSIM—Fortran programs for simulating ground motions from earthquakes: Version 2.3—a revision of U.S. Geol. Surv. Open-File Rept. OFR 96-80-A, *U.S. Geol. Surv. Open-File Rept. OF 00-509*, 55 pp.
- Boore, D. M., and G. M. Atkinson (2008). Ground-motion prediction equations for the average horizontal component of PGA, PGV, and 5%-damped PSA at spectral periods between 0.01 s and 10.0 s, *Earthq. Spectra* **24**, 99–138.
- Boore, D. M., and W. B. Joyner (1997). Site amplifications for generic rock sites, *Bull. Seismol. Soc. Am.* **87**, 327–341.
- Boore, D. M., W. B. Joyner, and L. Wennerberg (1992). Fitting the stochastic  $\omega^2$  source model to observed response spectra in western North America: Trade-offs between  $\Delta\sigma$  and  $\kappa$ , *Bull. Seismol. Soc. Am.* **82**, 1956–1963.
- Castro, R. R., H. Fabriol, M. Bour, and B. Le Brun (2003). Attenuation and site effects in the region of Guadeloupe, Lesser Antilles, *Bull. Seismol. Soc. Am.* **93**, 612–626.
- Cauzzi, C., and E. Faccioli (2008). Broadband (0.05 to 20 s) prediction of displacement response spectra based on worldwide digital records, *J. Seismology* **12**, no. 4, 453–475, doi [10.1007/s10950-008-9098-y](https://doi.org/10.1007/s10950-008-9098-y).
- Choi, Y., and J. P. Stewart (2005). Nonlinear site amplification as function of 30 m shear wave velocity, *Earthq. Spectra* **21**, 1–30.
- Crouse, C. B. (1991). Ground-motion attenuation equations for earthquakes on Cascadia subduction zone, *Earthq. Spectra* **7**, no. 2, 201–236.
- Dhakal, Y. P., N. Takai, and T. Sasatani (2008). Path effects on prediction equations of pseudo-velocity response spectra in northern Japan, *14th World Conference on Earthquake Engineering (WCEE)*, Beijing, China, 12–17 October 2008 (CD-ROM).
- Douglas, J. (2004). Ground motion estimation equations 1964–2003: Reissue of ESEE Report No. 01-1: "A comprehensive worldwide summary of strong-motion attenuation relationships for peak ground acceleration and spectral ordinates (1969 to 2000)" with corrections and additions, Tech. Rept. 04-001-SM: available from the Department of Civil and Environmental Engineering, Imperial College of Science, Technology and Medicine, London, U.K., at <http://www3.imperial.ac.uk/civilengineering/research/researchnewsandreports/researchreports> (last accessed January 2009).
- Douglas, J. (2006). Errata of and additions to "Ground motion estimation equations 1964–2003," Intermediary Rept. RP-54603-FR: available from Bureau de Recherches Géologiques et Minières (BRGM), Orléans, France, at <http://www.brgm.fr/publication/pubDetailRapportSP.jsp?id=RSP-BRGM/RP-54603-FR> (last accessed January 2009).

- Douglas, J. (2008). Further errata of and additions to "Ground motion estimation equations 1964–2003," Final Rept. RP-56187-FR, BRGM, Orléans, France.
- Earthquake Engineering Research Institute (EERI) (2006). The Kythira (Greece) earthquake of January 8, 2006: Preliminary report on strong motion data, geotechnical and structural damage, *EERI Newsletter* March 2006, **40**, no. 3, 1–21.
- Fukushima, Y. (1997). Comment on "Ground motion attenuation relations for subduction zones," *Seism. Res. Lett.* **68**, 947–949.
- García, D., S. K. Singh, M. Herráiz, J. F. Pacheco, and M. Ordaz (2004). Inslab earthquakes of central Mexico:  $Q$ , source spectra, and stress drop, *Bull. Seismol. Soc. Am.* **94**, 789–802.
- Goda, K., and H. P. Hong (2008). Spatial correlation of peak ground motions and response spectra, *Bull. Seismol. Soc. Am.* **98**, 354–365, doi [10.1785/0120070078](https://doi.org/10.1785/0120070078).
- Gregor, N., W. J. Silva, and I. G. Wong (2002). Ground-motion attenuation relationships for Cascadia subduction zone megathrust earthquakes based on a stochastic finite-fault model, *Bull. Seismol. Soc. Am.* **92**, no. 5, 1923–1932.
- Hatzfeld, D., G. Pedotti, P. Hatzidimitriou, D. Panagiotopoulos, M. Scordilis, J. Drakopoulos, K. Makropoulos, N. Delibasis, J. Latoussakis, J. Baskoutas, and M. Frogneux (1988). The Hellenic subduction beneath the Peloponnese: First results of a microearthquake study, *Earth Planet. Sci. Lett.* **93**, 283–291.
- Hatzidimitriou, P. M. (1995).  $S$ -wave attenuation in the crust waves of Northern Greece, *Pure Appl. Geophys.* **140**, 1381–1387.
- Jousset, P., and J. Douglas (2007). Long-period earthquake ground displacements recorded on Guadaloupe (French Antilles), *Earthq. Eng. Struct. Dyn.* **36**, 949–963.
- Kanno, T., A. Narita, N. Morikawa, H. Fujiwara, and Y. Fukushima (2006). A new attenuation relation for strong ground motion in Japan based on recorded data, *Bull. Seismol. Soc. Am.* **96**, 879–897.
- Karagianni, E. E., C. B. Papazachos, D. G. Panagiotopoulos, P. Suhadolc, A. Vuan, and G. F. Panza (2005). Shear velocity structure in the Aegean area obtained by inversion of Rayleigh waves, *Geophys. J. Int.* **160**, 127–143.
- Karakostas, C., T. Makarios, V. Lekidis, T. Salonikios, S. Sous, K. Makra, A. Anastasiadis, N. Klimis, P. Dimitriou, B. Margaris, C. Papaioannou, and N. Theodoulidis (2006). The Kythera (Greece) earthquake of January 8, 2006: Preliminary report on strong motion data, geotechnical and structural damage: available from Earthquake Engineering Research Institute at [http://www.eeri.org/lfe/pdf/greece\\_kythira\\_ITSAK.pdf](http://www.eeri.org/lfe/pdf/greece_kythira_ITSAK.pdf), 21 pp. (last accessed January 2009).
- Kiratzí, A., and C. B. Papazachos (1995). Active deformation of the shallow part of the subducting lithospheric slab in the southern Aegean, *J. Geodynamics* **19**, 65–78.
- Klimis, N. S., B. N. Margaris, and P. K. Koliopoulos (1999). Site-dependent amplification functions and response spectra in Greece, *J. Earthq. Eng.* **3**, 237–270.
- Konno, K., and T. Ohmachi (1998). Ground-motion characteristics estimated from spectral ratio between horizontal and vertical components of microtremor, *Bull. Seismol. Soc. Am.* **88**, 228–241.
- Konstantinou, I. K., I. S. Kalogeras, N. S. Melis, M. C. Kourouzidis, and G. N. Stavrakakis (2006). The 8 January 2006 Earthquake ( $M_w$  6.7) offshore Kythera Island, southern Greece: Seismological, strong-motion, and macroseismic observations of an intermediate-depth event, *Seism. Res. Lett.* **77**, 544–553.
- Kovachev, S. A., I. P. Kuzin, S. O. Yu, and S. L. Soloviev (1991). Attenuation of  $S$ -waves in the lithosphere of the Sea of Crete according to OBS observations, *Phys. Earth Planet. Int.* **69**, 101–111.
- Lee, C. T., and B. R. Tsai (2008). Mapping  $V_{530}$  in Taiwan, *Terr. Atmos. Ocean Sci.* **19**, 671–682, doi [10.3319/TAO.2008.19.6.671](https://doi.org/10.3319/TAO.2008.19.6.671)(PT).
- LePichon, X., and J. Angelier (1979). The Hellenic arc and trench system: A key to the neotectonic evolution of the eastern Mediterranean area, *Tectonophysics* **60**, 1–42.
- Macias, M., G. M. Atkinson, and D. Motazedian (2008). Ground-motion attenuation, source, and site effects for the 26 September 2003  $M$  8.1 Tokachi-Oki earthquake sequence, *Bull. Seismol. Soc. Am.* **98**, 1947–1963.
- Margaris, B. N., and D. M. Boore (1998). Determination of  $\Delta\sigma$  and  $\kappa_0$  from response spectra of large earthquakes in Greece, *Bull. Seismol. Soc. Am.* **88**, 170–182.
- Margaris, B. N., and P. M. Hatzidimitriou (2002). Source spectral scaling and stress release estimates using strong-motion records in Greece, *Bull. Seismol. Soc. Am.* **92**, 1040–1059.
- Nakamura, R., and T. Uetake (2000). Three dimensional attenuation structure and site amplification inversion by using a large quantity of seismic strong motion records in Japan, *12th World Conference on Earthquake Engineering (WCEE)*, Auckland, New Zealand, 30 January–4 February 2000, ID0724 (CD-ROM).
- National Earthquake Hazards Reduction Program (NEHRP) (1994). Recommended provisions for seismic regulations for new building and other structures, *Part 1: Provisions, FEMA 222A Building Seismic Safety Council*, Washington D.C., 290 pp.
- Oth, A., S. Parolai, D. Bindi, and F. Wenzel (2009). Source spectra and site response from  $S$  waves of intermediate-depth Vrancea, Romania, earthquakes, *Bull. Seismol. Soc. Am.* **99**, 235–254, doi [10.1785/0120080059](https://doi.org/10.1785/0120080059).
- Paolucci, R., A. Rovelli, E. Faccioli, C. Cauzzi, D. Finazzi, M. Vanini, C. Di Alessandro, and G. Calderoni (2008). On the reliability of long-period response spectral ordinates from digital accelerograms, *Earthq. Eng. Struct. Dyn.* **37**, 697–710.
- Papazachos, B. C., and P. E. Comninakis (1969). Geophysical features of the Greek island arc and Eastern Mediterranean ridge, *Seance de la Conference reunie a Madrid*, 1–12 September 1969, Comptes Rendus, 16, 74–75.
- Papazachos, B. C., and P. E. Comninakis (1971). Geophysical and tectonic features of the Aegean arc, *J. Geophys. Res.* **76**, 8517–8533.
- Papazachos, B. C., and N. D. Delibasis (1969). Tectonic stress field and seismic faulting in the area of Greece, *Tectonophysics* **7**, 231–255.
- Papazachos, C. B., and G. Nolet (1997).  $P$  and  $S$  deep velocity structure of the Hellenic area obtained by robust non-linear inversion of travel times, *J. Geophys. Res.* **102**, 8349–8367.
- Papazachos, B., and C. Papazachou (2003). *The Earthquakes of Greece*, Third Ed., Ziti Public, Thessaloniki, Greece, 286 pp.
- Papazachos, B. C., S. T. Dimitriadis, D. G. Panagiotopoulos, C. B. Papazachos, and E. E. Papadimitriou (2005). Deep structure and active tectonics of the Southern Aegean volcanic arc, in *Developments in Volcanology: The South Aegean Volcanic Arc*, M. Fytikas and G. Vougioukalakis (Editors), Elsevier, Amsterdam, 47–64, 391 pp.
- Papazachos, B. C., B. G. Karakostas, C. B. Papazachos, and E. M. Scordilis (2000). The geometry of the Wadati–Benioff zone and lithospheric kinematics in the Hellenic arc, *Tectonophysics* **319**, 275–300.
- Papazachos, B. C., E. E. Papadimitriou, A. A. Kiratzí, C. B. Papazachos, and E. K. Louvari (1998). Fault plane solutions in the Aegean sea and the surrounding area and their tectonic implications, *Boll. Geofis. Teor. Appl.* **39**, 199–218.
- Satoh, T. (2006). High-stress drop interplate and intraplate earthquakes occurred off shore of Miyagi Prefecture, Japan, in *3rd International Symposium on the Effects of Surface Geology on Seismic Motion*, P.-Y. Bard, E. Chaljub, C. Cornou, F. Cotton, and P. Gueguen (Editors), Grenoble, France, 30 August–1 September 2006, Laboratoire Central des Ponts et Chaussées, 689–698.
- Skarlatoudis, A. A., and B. N. Margaris (2006). Kythera 2006 earthquake: Data processing of strong motion from various digital sensors, *1st European Conf. on Earthquake Engineering and Seismology (ECEES)*, Geneva, Switzerland, 3–9 September 2006.
- Skarlatoudis, A. A., C. B. Papazachos, B. N. Margaris, N. Theodoulidis, Ch. Papaioannou, I. Kalogeras, E. M. Scordilis, and V. Karakostas (2003). Empirical peak ground motion predictive relations for shallow earthquakes in Greece, *Bull. Seismol. Soc. Am.* **93**, 2591–2603.
- Skarlatoudis, A. A., C. B. Papazachos, B. N. Margaris, C. Papaioannou, C. Ventouzi, D. Vamvakaris, A. Bruestle, T. Meier, W. Friederich, G. Stavrakakis, T. Taymaz, R. Kind, A. Vafidis, and T. Dahm

- the EGELADOS Group (2009). Combination of acceleration-sensor and broadband velocity-sensor recordings for attenuation studies: The case of the 8 January 2006 Kythera intermediate-depth earthquake, *Bull. Seismol. Soc. Am.* **99**, 694–704.
- Spakman, W. (1988). Upper mantle delay time tomography with an application to the collision zone of the Eurasian, African, and Arabian plates, *Ph.D. Thesis*, University of Utrecht, 53, 200 pp.
- Spakman, W., S. Van der Lee, and R. D. Van der Hilst (1993). Travel-time tomography of the European-Mediterranean mantle down to 1400 km, *Phys. Earth Planet. Int.* **79**, 3–74.
- Taymaz, T., J. Jackson, and R. Westaway (1990). Earthquake mechanisms in the Hellenic trench near Crete, *Geophys. J. Int.* **102**, 695–731.
- Theodulidis, N., and B. Papazachos (1990). Strong motion from intermediate depth subduction earthquakes and its comparison with that of shallow earthquakes in Greece, *Proc. of the XXII General Assembly European Seismological Commission*, Barcelona, Spain, 17–22 September 1990, II, 857–864.
- Uniform Building Code (1997). *International Building Officials USA*, Vol. **II**, 489 p.
- Wu, C. F., W. H. K. Lee, and D. M. Boore (2008). Strong-motion data from the two Pingtung, Taiwan, earthquakes of 26 December 2006, *Terr. Atmos. Ocean Sci.* **19**, 595–639, doi [10.3319/TAO.2008.19.6.595\(PT\)](https://doi.org/10.3319/TAO.2008.19.6.595(PT)).
- Youngs, R., S. Chiou, W. Silva, and J. Humphrey (1997). Strong ground motion attenuation relationships for subduction zone earthquakes, *Seism. Res. Lett.* **68**, 58–73.
- Zelimer, G. F. (1998). Petrogenetic processes and their time scales beneath Santorini, Aegean Volcanic arc, Greece, *Ph.D. Thesis*, Department of Earth Sciences, The Open University Milton Keynes, U.K.
- Zhao, J. X., J. Zhang, A. Asano, Y. Ohno, T. Oouchi, T. Takahashi, H. Ogawa, K. Irikura, H. K. Thio, P. G. Somerville, Y. Fukushima, and Y. Fukushima (2006). Attenuation relations of strong ground motion in Japan using site classification based on predominant period, *Bull. Seismol. Soc. Am.* **96**, 898–913.

U.S. Geological Survey  
345 Middlefield Road  
Menlo Park, California 94025  
boore@usgs.gov  
(D.M.B.)

Geophysical Laboratory  
University of Thessaloniki  
PO Box 352-1, GR-54124  
Thessaloniki, Greece  
askarlat@geo.auth.gr  
kpapaza@geo.auth.gr  
(A.A.S., C.B.P., C.V.)

Institute of Engineering Seismology and Earthquake Engineering (ITSAK)  
P.O. Box 53, GR 551 02 Finikas  
Thessaloniki, Greece  
margaris@itsak.gr  
(B.N.M.)

Manuscript received 7 August 2008